2018

Combination anti-Aβ treatment maximizes cognitive recovery and rebalances mTOR signaling in APP mice

Angie C.A. Chiang

Stephanie W. Fowler

Ricky R. Savjani

Susan G. Hilsenbeck

Clare E. Wallace

See next page for additional authors

Authors

Angie C.A. Chiang, Stephanie W. Fowler, Ricky R. Savjani, Susan G. Hilsenbeck, Clare E. Wallace, John R. Cirrito, Pritam Das, and Joanna L. Jankowsky

JEM Journal of Experimental Medicine

ARTICLE

Combination anti-Aβ treatment maximizes cognitive recovery and rebalances mTOR signaling in APP mice

Angie C.A. Chiang[1], Stephanie W. Fowler[1], Ricky R. Savjani[2], Susan G. Hilsenbeck[3], Clare E. Wallace[4], John R. Cirrito[4], Pritam Das[5], and Joanna L. Jankowsky[1,6]

Drug development for Alzheimer's disease has endeavored to lower amyloid β (Aβ) by either blocking production or promoting clearance. The benefit of combining these approaches has been examined in mouse models and shown to improve pathological measures of disease over single treatment; however, the impact on cellular and cognitive functions affected by Aβ has not been tested. We used a controllable APP transgenic mouse model to test whether combining genetic suppression of Aβ production with passive anti-Aβ immunization improved functional outcomes over either treatment alone. Compared with behavior before treatment, arresting further Aβ production (but not passive immunization) was sufficient to stop further decline in spatial learning, working memory, and associative memory, whereas combination treatment reversed each of these impairments. Cognitive improvement coincided with resolution of neuritic dystrophy, restoration of synaptic density surrounding deposits, and reduction of hyperactive mammalian target of rapamycin signaling. Computational modeling corroborated by in vivo microdialysis pointed to the reduction of soluble/exchangeable Aβ as the primary driver of cognitive recovery.

Introduction

Therapeutic development for Alzheimer's disease (AD) has largely focused on reduction of amyloid β (Aβ) peptide, by either inhibiting the enzymes required for Aβ production or promoting Aβ clearance using recombinant antibodies. To date, all Aβ-lowering clinical trials and most animal model studies have tested for functional improvement one approach at a time. Some in the field have responded to the limited success of this strategy by calling for combination treatments to be tested (Perry et al., 2015; Stephenson et al., 2015; Hendrix et al., 2016). This idea is supported by the benefits of polytherapy in other complex diseases such as cancer, tuberculosis, and HIV/AIDS (Günthard et al., 2016; Bayat Mokhtari et al., 2017; Kerantzas and Jacobs, 2017). We and others have shown that combination anti-Aβ treatments were better than single treatments at limiting plaque formation in mouse models of Alzheimer's amyloidosis (Chow et al., 2010; Wang et al., 2011; Jacobsen et al., 2014; Devi and Ohno, 2015). Yet only two of these studies initiated treatment after amyloid onset, and neither looked at the potential cognitive benefit of this strategy (Chow et al., 2010; Wang et al., 2011; Jacobsen et al., 2014; Devi and Ohno, 2015). Thus, although there may be mounting interest in multidrug therapy for AD, limited preclinical evidence is available to support its promise.

Here we endeavor to fill this knowledge gap. The central goal of our study was to test whether better Aβ abatement by combining anti-Aβ treatments resulted in better cognitive recovery. Secondary to this, we wanted to know what happened to neural markers in brain tissue that is cleared of Aβ, and further, whether we could identify signaling pathways that might connect the recovery of neuronal homeostasis with Aβ reduction. Our studies made use of an APP transgenic model in which the overexpression of pathogenic APP can be temporally controlled with doxycycline (dox; Jankowsky et al., 2005). Lowering APP expression in turn lowers Aβ production, and thus provides a pharmacogenetic mimic of chemical secretase inhibition. Although this is an artificial model, the approach avoided the known toxicities of commercially available secretase inhibitors that would have prevented prolonged treatment (Imbimbo and Giardina, 2011; Golde et al., 2013; De Strooper and Chávez Gutiérrez, 2015). Using this controllable APP model, we have previously shown that transgene suppression alone halts further amyloid formation but, when combined with passive anti-Aβ immunization, results in the clearance of up to 50% of deposited Aβ from the brain (Wang et al., 2011). Here we

[1]Department of Neuroscience, Baylor College of Medicine, Houston, TX; [2]Texas A&M Health Science Center, College Station, TX; [3]Department of Medicine, Lester and Sue Smith Breast Center, Dan L Duncan Comprehensive Cancer Center, Baylor College of Medicine, Houston, TX; [4]Department of Neurology, Knight Alzheimer's Disease Research Center, Hope Center for Neurological Disorders, Washington University School of Medicine, St. Louis, MO; [5]Department of Neuroscience, Mayo Clinic Florida, Jacksonville, FL; [6]Departments of Neurology, Neurosurgery, and Molecular and Cellular Biology, Baylor College of Medicine, Houston, TX.

Correspondence to Joanna L. Jankowsky: jankowsk@bcm.edu.

examine the impact of plaque removal versus maintenance on cognitive performance, cellular pathology, and biochemical alterations associated with Aβ accumulation. We then leverage this dataset to computationally model the relationship between Aβ concentration and behavioral performance with the goal of identifying which form of Aβ contributes most strongly to the effect of treatment.

Results

Combination therapy removes deposited Aβ and lowers soluble Aβ levels in transgenic mice

We used the tet-off APP transgenic mouse as a model for lowering Aβ production after disease onset. The tet-off APP mouse is based on the coexpression of two independent transgenes, one encoding the tetracycline transactivator (tTA) under control of the CaMKIIα promoter, the other encoding mutant APP under control of a tTA-responsive promoter. Intercrossing the two transgenic lines produces bigenic APP/TTA mice in which dox can be used to arrest expression of transgenic APP and subsequently reduce Aβ release. Dox treatment of APP/TTA mice thus provides a nontoxic chemogenetic mimic of secretase inhibition that is safe for long-term use.

Because our goal in the current study was to test whether the behavioral effect of Aβ suppression could be improved by adding passive anti-Aβ immunization, we needed to identify an age when transgene suppression alone would not fully rescue learning and memory impairments in this model. We had previously shown that short-term suppression of transgenic APP was sufficient to reverse cognitive deficits when started at the earliest sign of impairment after 6 mo of transgene expression (Fowler et al., 2014). Spatial learning and memory continued to decline with ongoing transgene expression (Chiang et al., 2018). By 9 mo, behavioral impairments were no longer rescued by the same dox treatment that had worked at 6 mo (Fig. S1). This age became the starting point for our current study.

Although dox-mediated control of transgenic APP was used to lower Aβ production, passive anti-Aβ immunization with mouse monoclonal IgG2a antibody Ab9 was used to sequester Aβ after its release (Levites et al., 2006a). Aged APP/TTA mice were divided into five experimental groups: pretreatment, vehicle, dox only, Ab9 only, or dox + Ab9 (Fig. 1 A). A total of 131 APP/TTA bigenic mice and 19 TTA single transgenic sibling controls were used. Mice in the pretreatment group provided baseline measures for the APP/TTA model before intervention and were used as a standard for comparison of treatment efficacy. All remaining animals were injected weekly with Ab9 (500 µg, i.p.) or vehicle. Mice in the dox-only and dox + Ab9 groups were fed chow containing 100 mg/kg dox. We ascertained by Western blot that transgenic APP expression was unchanged by Ab9 or vehicle injection but effectively reduced by >95% at this dose in both dox-treated groups (Fig. 1 B). The pretreatment group was behaviorally tested without treatment and harvested 3 wk later. All other groups were behaviorally tested after 9 wk of differential treatment and harvested after 12 wk.

We first examined the effect of treatment on plaque burden in the brain. Based on past characterization, we expected and confirmed that pretreatment animals harbored significant plaque pathology throughout the forebrain (44% surface area in cortex and 25% in hippocampus as measured by silver staining; Fig. 2, A and D; and Fig. S2). Vehicle-treated mice continued to accumulate Aβ deposits over the next 12 wk and were harvested with 73% of the cortex and 49% of the hippocampus involved. Antibody alone had little impact, whereas dox-mediated APP suppression maintained plaque load at pretreatment levels (43% cortex and 23% hippocampus). The combination of dox + Ab9 significantly lowered plaque burden by ∼40% relative to pretreatment, leaving a footprint of just 26% area in the cortex and 14% in hippocampus (see Table S1 for statistics). This change demonstrated that the impact of immunotherapy could be amplified by concurrently targeting Aβ production, and conversely, that plaque clearance occurs only when stimulated by anti-Aβ antibodies.

We next examined the distribution of oligomeric Aβ using monoclonal antibody NAB61 (Lee et al., 2006). NAB61 immunoreactivity occupied considerably less surface area than silver stain, but relative differences between treatment groups remained. Compared with pretreatment, the vehicle group had significantly more NAB61 immunostaining at harvest, whereas the dox + Ab9 group had significantly less (Fig. 2, B and E; Fig. S2; and Table S1). NAB61 immunoreactivity did not change significantly from pretreatment in either monotherapy group. Fibrillar amyloid detected by thioflavin-S rose significantly in both vehicle and Ab9 groups but was held to pretreatment levels in dox-only mice. Unlike the Aβ deposits detected by silver stain and NAB61, thioflavin-positive plaques were not reduced by combination treatment (Fig. 2, C and F; Fig. S2; and Table S1). These results are consistent with past work in younger APP/TTA mice and confirm that the chemogenetic arrest of Aβ release permits clearance of diffuse deposits but not fibrillar cores by concurrent administration of effector-competent anti-Aβ antibody (Wang et al., 2011).

In parallel with histological measures of plaque burden, we also assessed Aβ concentration by ELISA in a subset of 15 mice from each condition using a three-step extraction method (Youmans et al., 2011). The most soluble Aβ extracted into TBS was most significantly affected by treatment. Both dox and dox + Ab9 groups had less TBS-soluble total Aβ than pretreatment, and within this extract, both $Aβ_{40}$ and $Aβ_{42}$ were significantly decreased (Fig. S3 and Table S1). No differences in TBS-X detergent-soluble Aβ were noted for any treatment group, whereas the only significant changes noted in guanidine-soluble Aβ were increases in the vehicle and Ab9-only groups, likely indicative of elevated fibrillar amyloid in these conditions (Fig. S3).

Recovery of synaptic markers in the plaque boundary area

Exposure to soluble oligomeric Aβ can induce reversible spine loss in hippocampal neurons (Calabrese et al., 2007; Lacor et al., 2007; Shankar et al., 2007), and we were curious to test whether synaptic markers would recover with oligomer reduction in vivo. Immunostaining for NAB61 suggested that the highest concentration of oligomeric Aβ occurred in immediate proximity to fibrillar plaques (Koffie et al., 2009; Chiang et al., 2018), so we focused our synaptic marker measurements on a 30-µm zone surrounding thioflavin-stained cores.

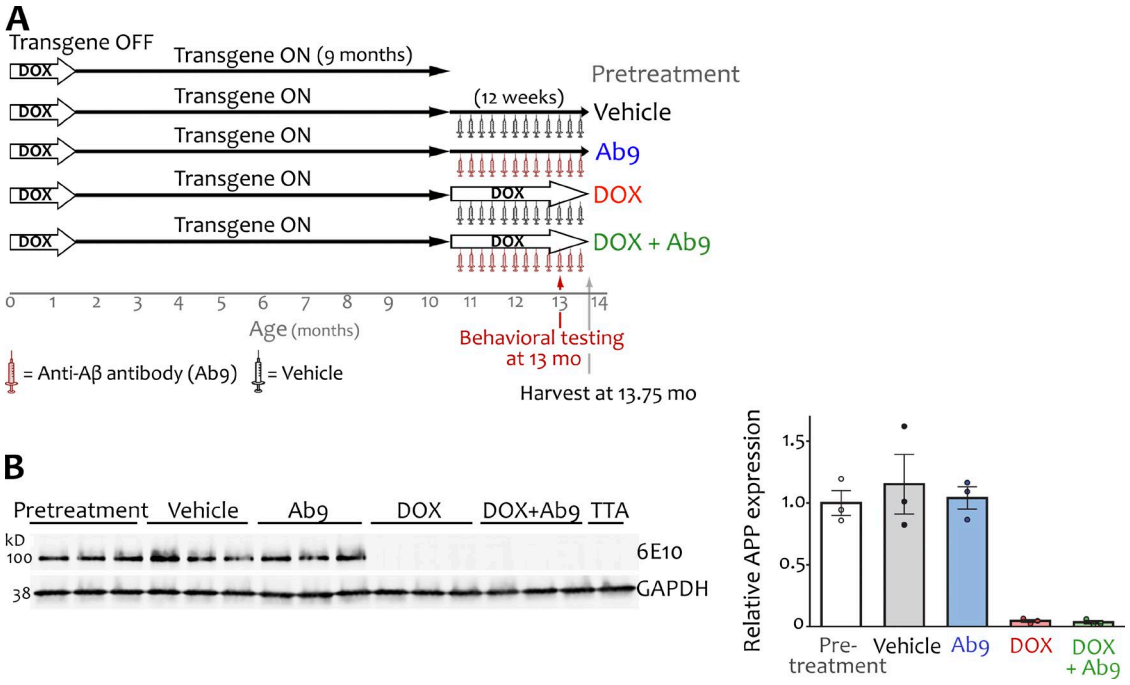

Figure 1. **Experimental design comparing the outcome of no treatment, passive immunization, transgene suppression, or both against performance before intervention. (A)** APP/TTA mice expressed transgenic APP for 9 mo (from 1.5 until 10.5 mo of age) before being divided into five experimental groups. Animals in the pretreatment group underwent immediate behavioral testing without intervention to measure baseline performance (n = 24). All other animals were treated for 12 wk with one of the following: vehicle (n = 28), Ab9 anti-Aβ antibody (n = 26), dox (n = 27), or dox + Ab9 (n = 26). Behavioral testing began 9 wk into each treatment and continued until animals were harvested for histological and biochemical analysis. **(B)** Western blot probed with human-specific antibody 6E10 confirmed effective transgene suppression in the dox-treated groups. Graph shows quantitation of APP signal relative to GAPDH for each lane and normalized to the pretreatment group mean. Error bars show means ± SEM.

We used a custom Matlab script to outline thioflavin plaques and measure the area of PSD-95 or synaptophysin immunofluorescence in three successive 10-µm-wide annuli. Quantification of PSD-95 was hindered by what appeared to be glial cells outlined in signal located adjacent to a subset of plaques in all treatment conditions (unpublished data). The variance in area measure introduced by this labeling made quantitation of PSD95 signal unreliable without manually selecting plaques for inclusion and exclusion. Synaptophysin immunofluorescence was more consistent and could be readily measured in an unbiased manner using an automated script. Differences between treatment groups were small but steady. The area of synaptophysin staining increased with distance from the plaque core for all treatment conditions, consistent with the idea that synaptotoxic peptide is most concentrated in the zone immediately adjacent to the core (Dong et al., 2007; Koffie et al., 2009; Dorostkar et al., 2014). Compared with pretreatment, however, a persistent increase of synaptophysin signal at all distances was observed only for animals treated with dox + Ab9 (Fig. 3 and Table S1).

Combination treatment lessens axonal swelling and rebalances a master lysosomal control

On seeing that combination treatment maximized synaptophysin as a marker of synaptic integrity in the area surrounding plaques, we wondered whether other neuronal pathologies associated with fibrillar Aβ deposits might also be attenuated. Dystrophic neurites are prominent in the immediate vicinity of fibrillar plaques, swollen with aggregated proteins and interrupted vesicles that interfere with electrical transmission and cargo trafficking (Knowles et al., 1999; Stern et al., 2004; Tsai et al., 2004; Stokin et al., 2005). Ubiquitinated proteins accumulate in these swellings along with markers of endoplasmic reticulum, and ubiquitin or reticulon immunostaining has been used to identify dystrophic neurites surrounding amyloid plaques (Dickson et al., 1990; Sharoar et al., 2016). Ubiquitin-filled neurites formed halos outlining presumptive plaques in APP/TTA mice before treatment and remained prominent in both untreated mice and those given Ab9 alone (Fig. 4 A). Compared with pretreatment, the area occupied by ubiquitin immunostain was significantly reduced by 32% in dox-treated animals and by 41% in mice given dox + Ab9 (Fig. 4, A and B). Similarly, LAMP1 is also highly enriched in dystrophic neurites and absent in normal adjacent structures, making it a good marker for detection of axonal swellings (Condello et al., 2011, 2015). LAMP1 immunofluorescence consistently surrounded thioflavin-S$^+$ amyloid cores in pretreatment animals. Compared with pretreatment, the extent of LAMP1 staining was reduced by 64% in mice given dox + Ab9 (Fig. 4, C and D; and Table S1). The area of LAMP1 immunostaining across the cortex was also lowered by dox alone, but the difference did not reach significance. These findings suggest that by removing diffuse aggregates of extracellular Aβ, pathological accumulation of intraneuronal protein can also be dismantled.

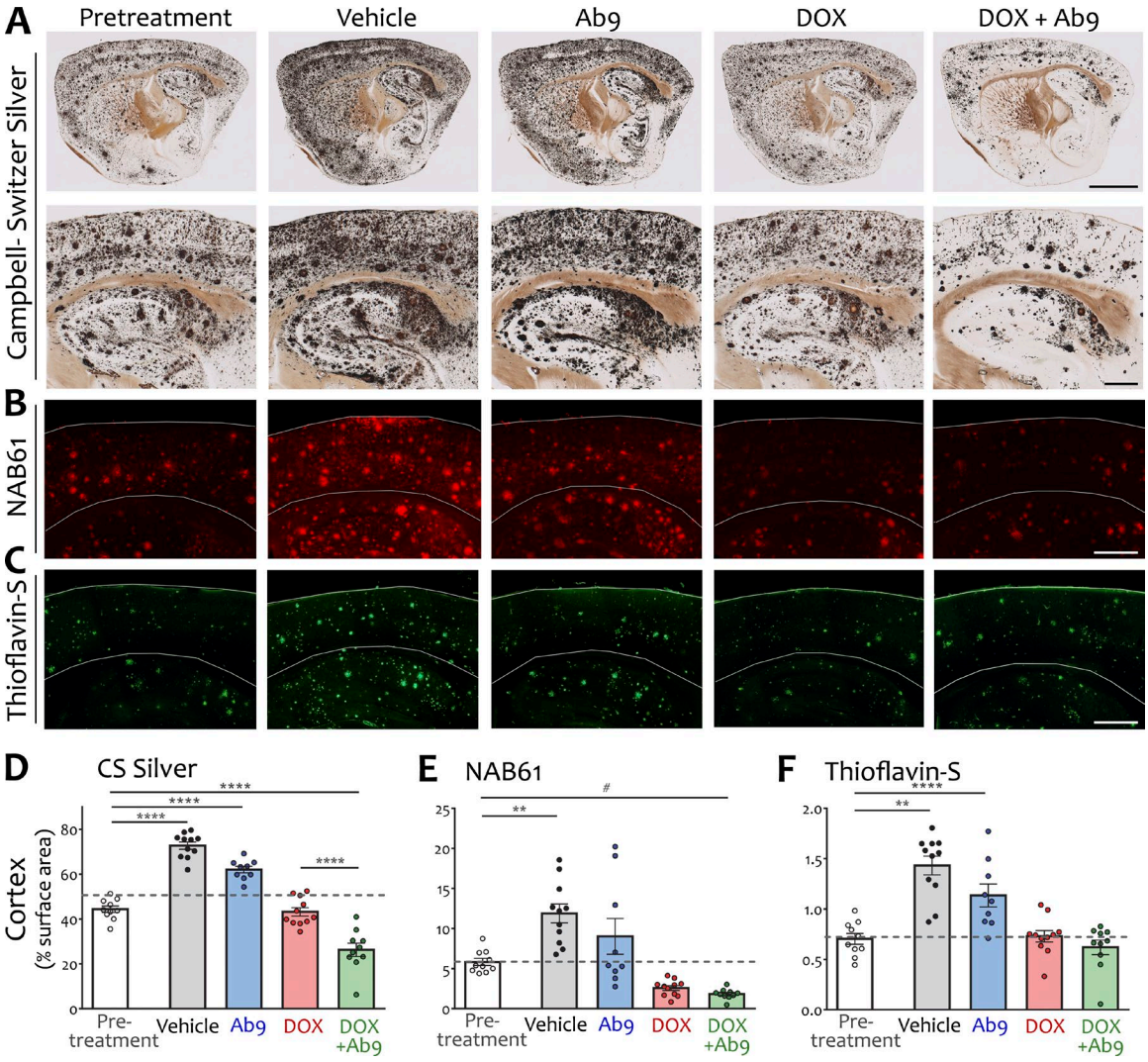

Figure 2. **Transgene suppression stopped further plaque formation; adding anti-Aβ antibody promoted plaque clearance. (A)** Sagittal sections stained by the Campbell–Switzer method reveal total plaque load in each treatment condition. Bottom row shows higher-magnification images centered on hippocampus and overlying cortex. Bars: (top row) 2,000 µm; (bottom row) 500 µm. **(B)** NAB61 immunofluorescence for oligomeric Aβ in dorsal hippocampus and overlying cortex. Gray lines indicate location of pial surface and corpus callosum. Bar, 500 µm. **(C)** Thioflavin-S stain for fibrillar amyloid in dorsal hippocampus and overlying cortex. Bar, 500 µm. **(D–F)** Quantification of cortical plaque area: CS silver (D), NAB61 (E), and thioflavin-S (F). Dashed line in scatter plots indicates the pretreatment plaque load for each stain. Significant comparisons against pretreatment or between dox and dox + Ab9 are shown; other comparisons are listed in Table S1. *n* = 9–11/group. **, P < 0.01; ****, P < 0.0001; #, P = 0.09. Error bars show means ± SEM.

Upstream of LAMP1, lysosomal biogenesis is regulated by the transcription factor EB (TFEB; Sardiello et al., 2009; Settembre et al., 2011). Accumulation of lysosomal proteins such as LAMP1 is consistent with defective autophagy in AD (Nixon, 2007; Nixon and Yang, 2011), and increased levels of TFEB have been documented in aged APP/PS1 mice (Zhang and Zhao, 2015). We found that unlike LAMP1, TFEB immunostaining labeled cells broadly across the cortex. The signal appeared to be cytoplasmically localized in all treatment conditions but less intensely stained in tissue from mice treated with dox or dox + Ab9 (Fig. 4 E). We confirmed this difference by Western blotting. Cortical expression of TFEB was elevated roughly 50% in pretreatment APP/TTA mice compared with TTA single transgenic siblings. TFEB expression was diminished by dox alone, but only dox + Ab9 reached significance versus pretreatment (Fig. 4, F and G; and Table S1).

Aberrant mTOR signaling as a common mediator of neuronal pathology rescued by combination therapy

Although innumerable signaling pathways have been implicated downstream of Aβ, the mTOR pathway stood out as a mediator capable of influencing both synapse density and lysosomal/autophagy function via a complex network of effector proteins (Garza-Lombó and Gonsebatt, 2016). mTOR hyperactivity has been detected in human AD brains and APP transgenic mice and can be induced by Aβ in wild-type mice (An et al., 2003; Griffin et al., 2005; Caccamo et al., 2010, 2011). We wondered whether hyperactive mTOR signaling might contribute to the synaptic and cellular phenotypes of untreated APP/TTA mice, and whether treatment would restore normal activity through this pathway. We used the phosphorylation of downstream target S6 ribosomal protein (p-$S6_{s420/244}$) as a readout for raptor-dependent mTORC1

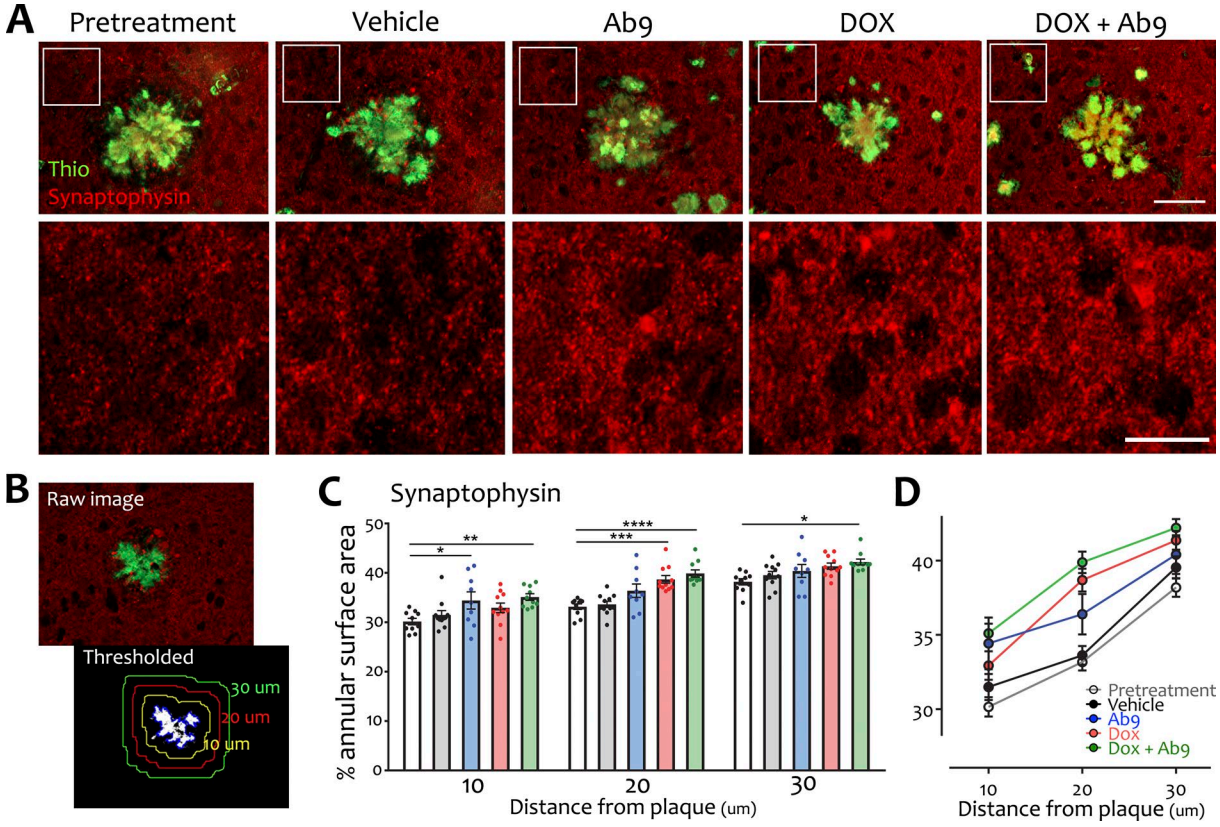

Figure 3. **Synaptic recovery surrounding amyloid cores after combination anti-Aβ treatment. (A)** Synaptophysin immunofluorescence (red) was measured in a zone immediately surrounding fibrillar plaques identified by thioflavin-S (green; top row). A magnified portion of the synaptophysin immunofluorescence (outlined in top row) is shown at higher magnification in the bottom row of images. Bars: (top row) 50 µm; (bottom row) 20 µm. **(B)** Illustration of image processing for area quantitation. Raw fluorescence images were converted to black and white for each color channel. The thresholded thioflavin image was used to outline the plaque, and this outline was expanded to delineate concentric rings that were applied to the thresholded synaptophysin image. **(C and D)** The area of synaptophysin staining was measured in concentric rings 0–10, 10–20, and 20–30 µm from the plaque edge. Graphs show individual scatter (C) and group mean (D) at each distance. Significant comparisons against pretreatment are shown; other comparisons are listed in Table S1. *n* = 9–11/group. *, P < 0.05; **, P < 0.01; ***, P < 0.001; ****, P < 0.0001. Error bars show means ± SEM.

activity and AKT/protein kinase B ($p\text{-}AKT_{s473}$) as a readout for rictor-dependent mTORC2 activity (Hoeffer and Klann, 2010; Costa-Mattioli and Monteggia, 2013). Immunoblotting of hippocampal extracts revealed a modest 1.5-fold increase of mTORC1 activity in pretreatment compared with TTA controls (Fig. 5, A and B), alongside an eightfold increase of mTORC2 activity (Fig. 5, C and D). The activity of both complexes was restored to control levels in mice treated with dox + Ab9 (Fig. 5, A–D; and Table S1). mTOR activity was nonsignificantly reduced in dox-treated animals and was unchanged in mice given vehicle or Ab9 alone.

mTORC2 signaling is known to regulate spine turnover in the adult brain via cofilin-dependent stabilization of synaptic actin. We explored this connection by immunoblotting hippocampal extracts for mTORC2-depedent cofilin phosphorylation ($p\text{-}cofilin_{s3}$; Huang et al., 2013). We detected hyperphosphorylation in the pretreatment group—consistent with elevated mTORC2 activity—that was significantly decreased in mice receiving either dox or dox + Ab9 and restored to the level of TTA controls in the latter group (Fig. 5, E and F; and Table S1). Thus, mTOR activity may mediate both the synaptic recovery (via mTORC2) and the resolution of lysosomal blockade (via mTORC1) that accompany cognitive recovery by combination therapy.

Combination treatment rescues cognitive function in aged transgenic mice

Our analyses so far showed that combination anti-Aβ therapy cleared diffuse amyloid, increased synapse area, resolved neuritic dystrophy, and normalized mTOR signaling. However, the primary goal of our study was to determine whether these effects of combined anti-Aβ treatment supported a better behavioral outcome than single interventions. To address this question, all animals underwent behavioral testing starting 9 wk into the 12-wk treatment period to measure the cognitive impact of each strategy. TTA single transgenic siblings were included as controls and were given either vehicle or dox + Ab9 on the same schedule as APP/TTA mice. We observed no significant differences between these two TTA treatment groups for any outcome measure (unpublished data), and so they were combined for illustration here. All animals underwent basic locomotor assessment before cognitive testing and visual acuity testing afterward; no significant impairments were detected in any group (Fig. S4).

Cognitive testing consisted of three tasks performed in succession to examine different aspects of hippocampal-dependent learning and memory. Testing began with a train-to-criteria version of the Morris water maze (MWM) that measured spatial

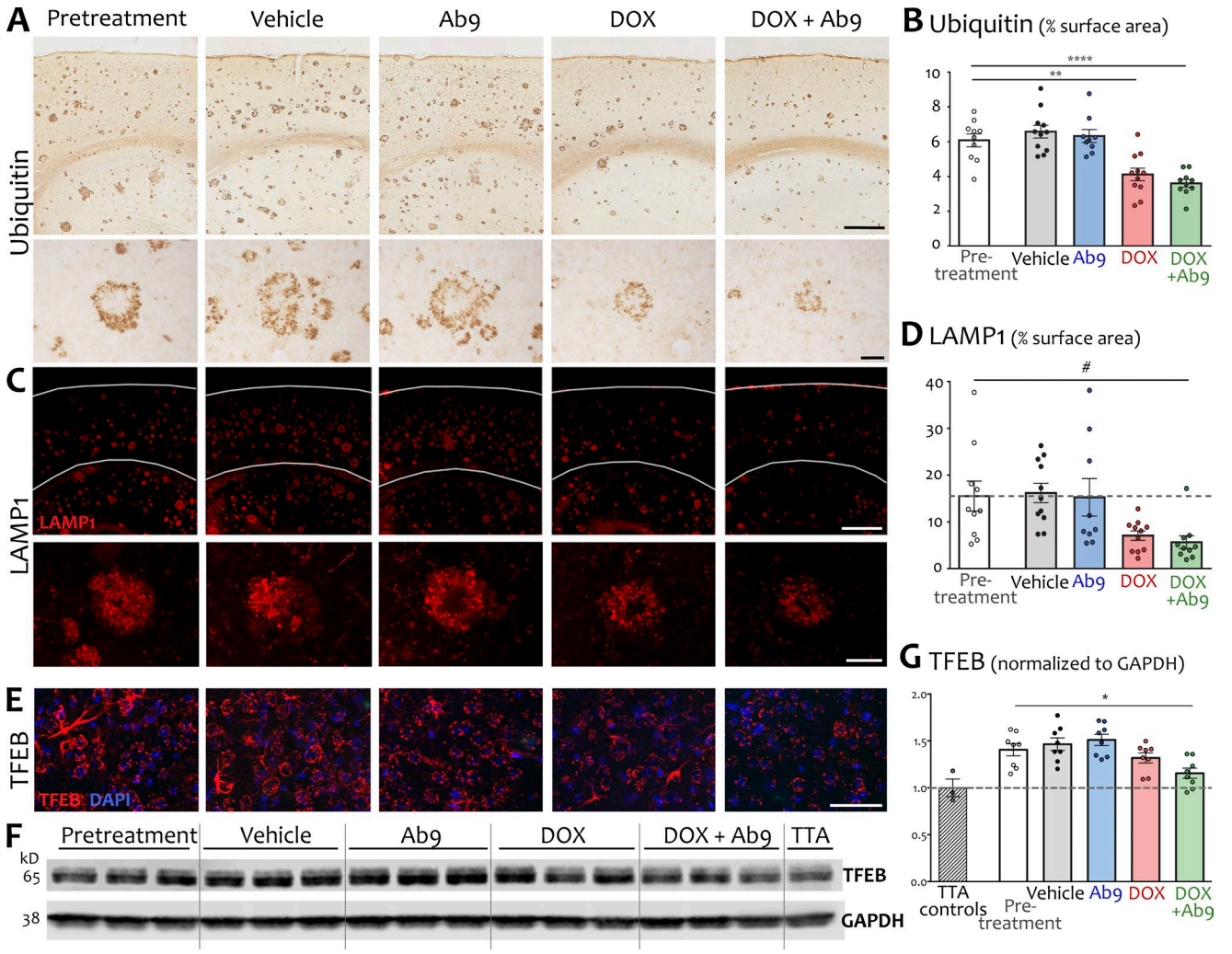

Figure 4. **Therapeutic reduction of extracellular Aβ allowed clearance of intraneuronal pathology. (A)** Representative images of ubiquitin immunohistochemistry for dystrophic neurites. Top row shows immunostaining in cortex and dorsal hippocampus at low magnification. Higher-magnification images (bottom row) show a single neuritic plaque to illustrate the remediation of neuritic swellings with dox and dox + Ab9 treatment. Bars: (top row) 500 µm; (bottom row) 50 µm. **(B)** Quantification of ubiquitin immunostaining as percent of cortical surface area. Dashed line indicates mean area of ubiquitin signal in pretreatment animals. **(C)** Representative immunofluorescence for the lysosomal marker LAMP1. Top row shows immunostaining in cortex and dorsal hippocampus at low magnification. Gray lines indicate rough location of pial surface and corpus callosum. Higher-magnification images (bottom row) show LAMP1 signal surrounding a single representative plaque in each condition. Bars: (top row) 500 µm; (bottom row) 50 µm. **(D)** Quantification of LAMP1 immunostaining as percent of cortical surface area. Dashed line indicates mean area of LAMP1 signal in pretreatment animals. **(E)** TFEB immunofluorescence (red) was not localized to plaques but appeared diffusely throughout the cortex, with lower signal intensity in dox and dox + Ab9 groups. Bar, 50 µm. **(F)** Representative Western blot for hippocampal TFEB expression. **(G)** Quantification of TFEB Western blots, expressed relative to GAPDH n = 8/group (3 for TTA). Dashed line in scatter plot indicates normalized mean TFEB expression in TTA control animals. TTA values in this and subsequent figures are for illustration only; statistical comparisons included only APP/TTA groups. Post hoc comparisons against pretreatment are shown; other post hoc comparisons are listed in Table S1. n = 9–11/group for histological analysis and n = 8/group for protein analysis. *, P < 0.05; **, P < 0.01; ****, P < 0.0001; #, P = 0.054. Error bars show means ± SEM.

reference learning and memory. This was followed by radial arm water maze (RAWM) to measure working memory and ended with contextual fear conditioning (FC) to measure associative memory. In each of these tasks, performance of the pretreatment group was markedly impaired compared with TTA controls, confirming that the APP/TTA mice displayed substantial cognitive deficits before intervention (Fig. 6, A, C, and D). The comparisons in which we were most interested, however, were not between genotypes but between treatment conditions, and specifically between the pretreatment and posttreatment groups. From this perspective, only mice given dox + Ab9 improved significantly across all three tasks compared with pretreatment performance, as described in detail below (Fig. 6, A–D; and Table S1).

We chose a train-to-criteria version of MWM so that we could distinguish learning from recall, and where relevant, test treatment effects on both. In this task, the rate of learning is measured by the number of days required to reach a preset performance level in probe trials conducted at the end of each training session. Dox + Ab9 was the only posttreatment group that took significantly fewer days to reach criterion performance than pretreatment (Fig. 6 A and Table S1). Despite their residual fibrillar pathology, dox + Ab9 mice learned this task as quickly as TTA controls. Dox + Ab9 was also the only group that showed faster

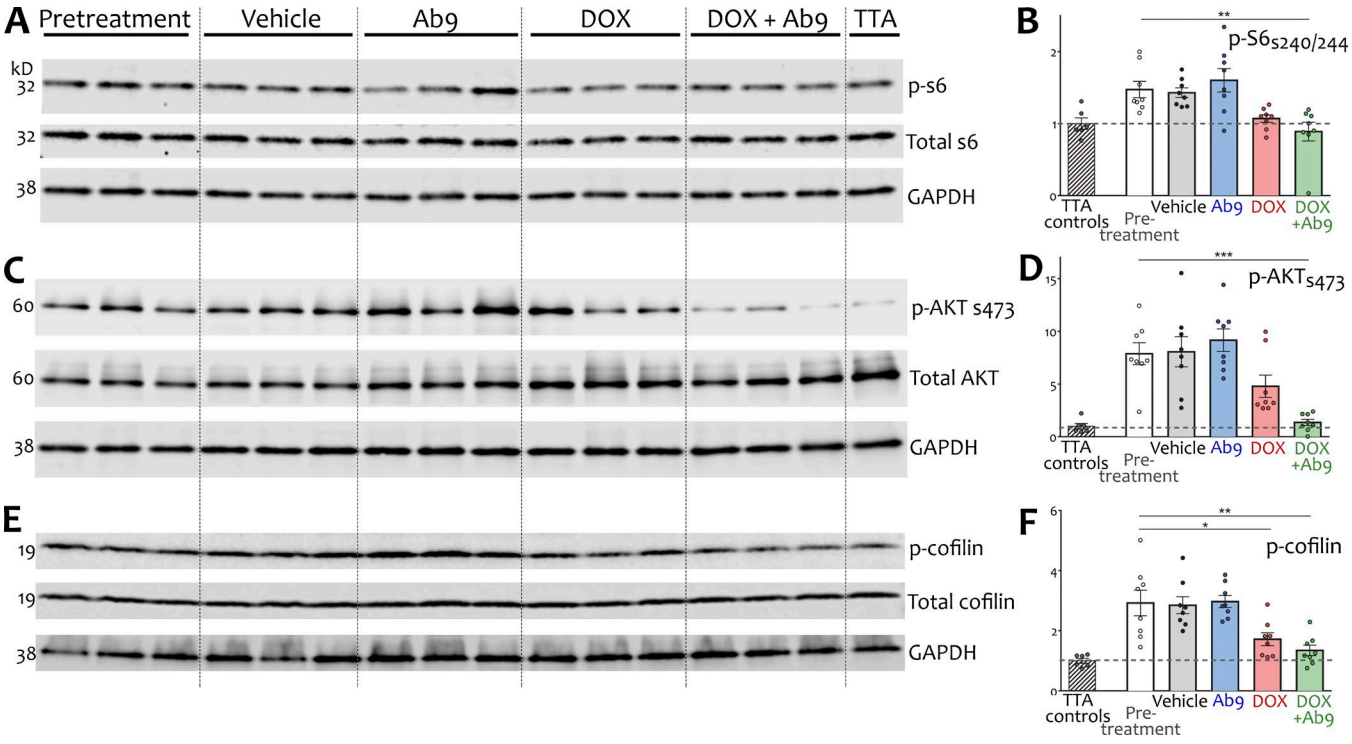

Figure 5. **Hyperactive mTOR signaling was normalized by combination anti-Aβ treatment. (A and B)** Representative Western blots and quantitation for hippocampal mTORC1-dependent phosphorylation of S6 ribosomal protein. **(C and D)** Western blots and quantitation for mTORC2-dependent phosphorylation of protein kinase B, also known as Akt. Note the *y*-axis scale in D, reflecting the dramatic elevation of mTORC2 activity in pretreatment APP/TTA mice compared with TTA controls. **(E and F)** Western blots and quantitation for cofilin phosphorylation downstream of mTORC2. Measurements are expressed as a ratio of phosphorylated to total protein for each marker. *n* = 8/group (6 for TTA). Dashed line in scatter plots indicates normalized mean expression in TTA control animals. Comparisons against pretreatment are shown; other post hoc comparisons are listed in Table S1. *, P < 0.05; **, P < 0.01; ***, P < 0.001. Error bars show means ± SEM.

improvement than pretreatment in their recall accuracy for the platform location during end-of-day probe trials (Fig. 6 B). In contrast, animals given dox alone appeared to be better than pretreatment, but post hoc comparisons never reached significance. This distinction suggests that dox + Ab9 afforded some functional benefit for spatial learning over dox alone, albeit not sufficient to reach statistical significance.

Once all mice in the testing group reached criteria performance in the MWM, the entire cohort was given refresher training and then tested for long-term memory 24 h later. This design ensures that all mice are at the same performance level before testing long-term spatial memory. Even at this advanced stage of pathology, we found no differences in long-term memory between genotypes (APP/TTA vs. TTA) or between treatment groups (Fig. S4 and Table S1). This outcome indicates that the primary spatial deficit of APP/TTA mice at this age is in learning and not recall.

We then reconfigured the pool to a six-arm radial maze as a 1-d test of working memory (modified from Alamed et al., 2006). In this task, incorrect arm entries represent an error of working memory, and the number of errors should decrease over successive trials as animals learn the maze (Fig. 6 C). The total number of arm entry errors for the day therefore serves as an aggregate measure of learning for this task. Compared with the pretreatment group, total entry errors was significantly reduced only for mice receiving dox + Ab9 (Fig. 6 C and Table S1).

We also examined the effect of anti-Aβ treatment on contextual FC. In this task, associative memory for an environment in which animals were mildly foot-shocked can be measured by the percentage of time they spend immobile when returned to the chamber the next day. Consistent with the findings from MWM and RAWM, only the dox + Ab9 group spent significantly more time immobile in the trained context than pretreatment (Fig. 6 D and Table S1).

Of note, mice given Ab9 or dox alone showed no significant improvement from pretreatment in any task (Fig. 6, A–C). Animals given dox alone showed a trend toward improvement in MWM and RAWM, but post hoc comparisons against pretreatment performance never reached significance. Because performance of the dox group against pretreatment often approached significance but always failed to reach P < 0.05 after adjustment for multiple comparisons, we were curious whether direct assessment of dox versus dox + Ab9 might support or refute the benefit of combination treatment. We wanted this analysis to capture overall performance and so used a multivariate ANOVA that incorporated behavioral outcomes from each task: days to criteria in MWM, total errors in RAWM, and percentage of time immobile in FC. This comparison of aggregate behavioral performance between dox and dox + Ab9 demonstrated a significant difference between groups (multivariate ANOVA, Wilk's $\Lambda = 0.812$, partial $\eta^2 = 0.19$; Table S1). On the whole, animals receiving combination therapy had indeed outperformed those receiving dox alone.

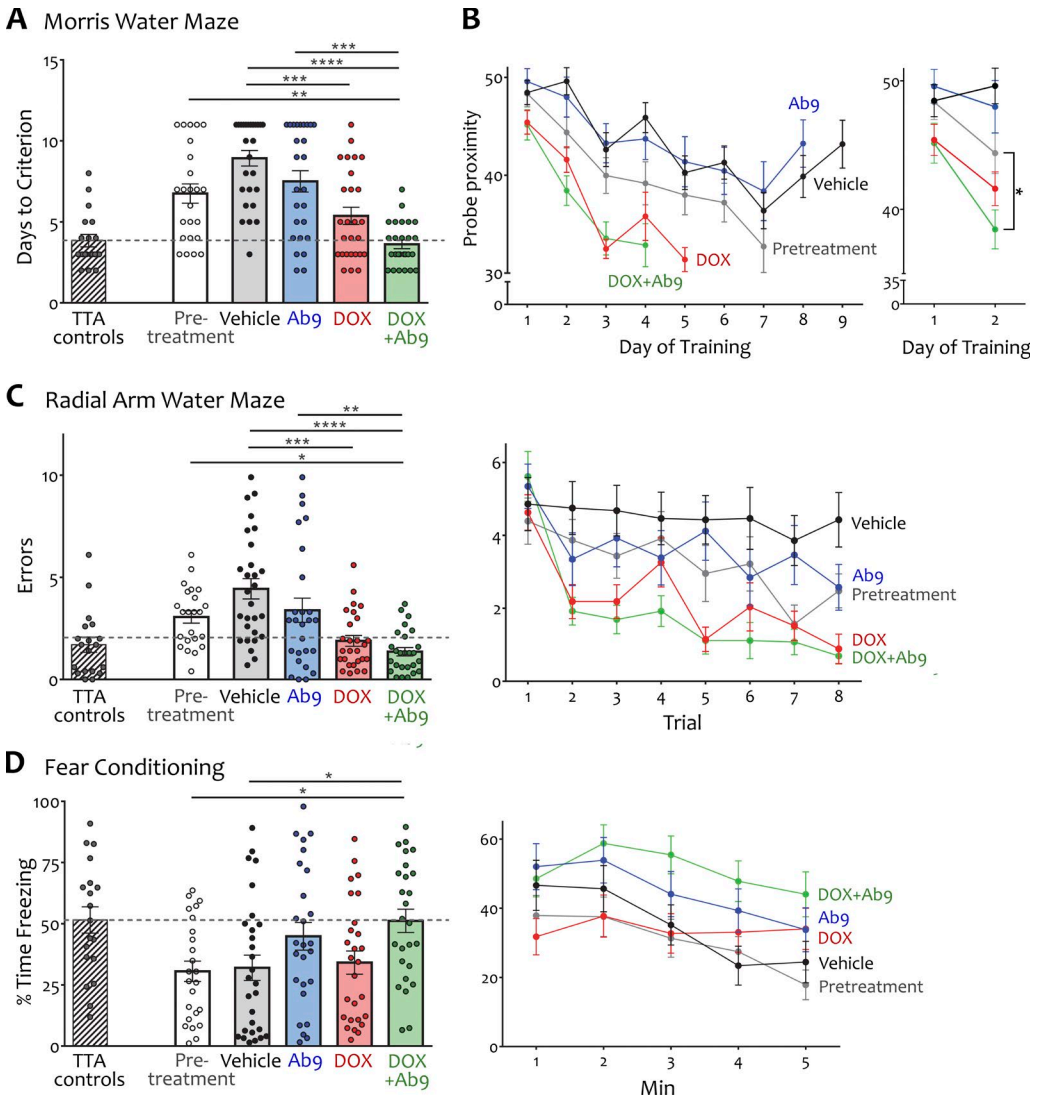

Figure 6. **Cognitive deficits in aged APP/TTA mice were rescued by combination anti-Aβ treatment. (A)** Mean number of training days to reach criteria performance in the MWM. **(B)** Proximity to trained location during MWM daily probe trials, plotted for the mean number of days to criteria performance for each group (left). Statistical comparison of improvement in MWM probe proximity between groups was tested for days 1–2 of training (right). **(C)** RAWM performance plotted as mean reentry errors per group (left) or by trial (right). **(D)** Percentage of time immobile during recall of contextual fear plotted as overall mean per group (left) or by minute (right). Dashed line in scatter plots of A, C, and D indicates mean performance of age-matched TTA mice. TTA values shown here are combined for vehicle and dox + Ab9 treatment and are not included in statistical comparisons of APP/TTA treatment groups. *n* = 24–28/group (19 for TTA). *, P < 0.05; **, P < 0.01; ***, P < 0.001; ****, P < 0.0001. Error bars show means ± SEM.

Reduction of soluble Aβ corresponds with improved behavioral performance

We realized that the dataset generated from our study might allow us to identify which forms of Aβ were most highly correlated with behavioral impairment across treatments and therefore would be most important to target for functional recovery. We began by examining simple Pearson correlations between the six Aβ concentrations measured by ELISA for each animal (Aβ 40 and 42 measured from TBS, TBSX, and guanidine extracts) and the four representative behavioral measures from MWM, RAWM, and FC. The behavioral outcomes included (a) MWM total daily mean path length to the platform during training, a continuous variable reflecting the rate at which animals learned the escape location; (b) MWM day 2 probe proximity, reflecting short-term memory performance on the final day that all animals were still in training; (c) RAWM mean errors, reflecting working memory performance, and (d) FC mean percentage time immobile, reflecting associative recall performance. Pearson testing revealed nominally significant correlations between Aβ concentration and the two spatial navigation tasks (MWM and RAWM) but found no significant relationship between Aβ and FC for either peptide in any extract (Table S1). We used these results to focus computational modeling on MWM and RAWM performance as a function of Aβ concentration in each animal. General linear models for MWM or RAWM outcomes were built with all six Aβ measures as possible independent variables, using forward and backward stepwise selection to minimize the Akaike information criterion. This unbiased optimization resulted in models that consistently included either TBS Aβ40 or TBS Aβ42 (which were highly collinear), along with one other nonoverlapping variable.

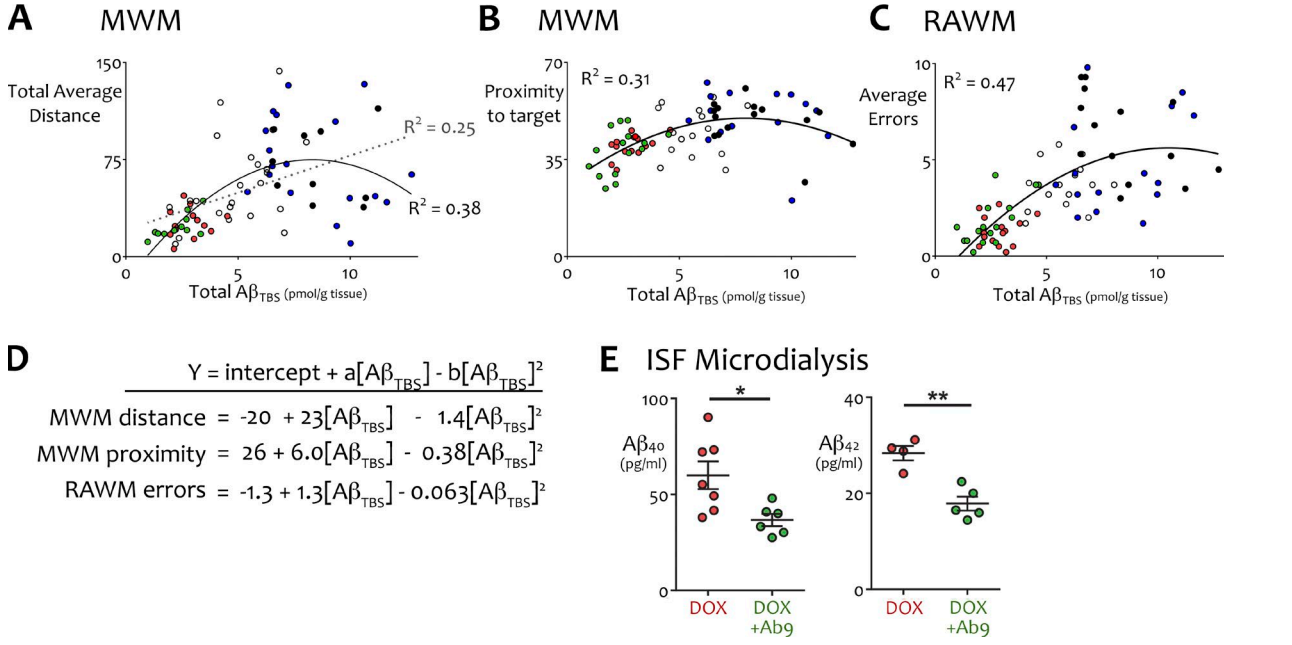

Figure 7. **TBS-soluble Aβ emerged as the primary driver of behavioral performance. (A–D)** MWM and RAWM performance modeled as a function of total cortical TBS-soluble Aβ. Values are plotted for every animal in which Aβ concentration was measured by ELISA after behavioral testing. Treatment groups are color coded: pretreatment (white), vehicle (black), Ab9 (blue), dox (red), dox + Ab9 (green). **(A)** Total daily mean distance to the platform (m) for all days of MWM training as a function of $A\beta_{TBS}$. Both linear (dotted line) and polynomial models (solid line) are shown for this dataset. R^2 values improved substantially with the addition of a second-order term. **(B)** Proximity to the trained location on the day 2 probe trial as a function of $A\beta_{TBS}$. **(C)** Mean arm reentry errors during trials 2–8 in RAWM as a function of $A\beta_{TBS}$. **(D)** Polynomial equations graphed in A–C. **(E)** Hippocampal ISF $A\beta_{40}$ and $A\beta_{42}$ measured by microdialysis in a subset of behaviorally tested mice (n = 6–7/group for Aβ40, n = 4–5/group for Aβ42). *, P < 0.05; **, P < 0.01. Error bars show means ± SEM.

In one case, this second variable did not contribute significantly to the final equation; in another it contributed negatively to the correlation. We therefore focused subsequent modeling on testing the extent to which TBS Aβ alone accounted for MWM and RAWM performance. Remarkably, we found that models based solely on total TBS Aβ fitted the behavioral data as well as the initial multivariate equations. Further graphical examination of the model residuals suggested that the relationship between behavior and TBS Aβ may be nonlinear. Each computational model was then modified to include a polynomial term. This modification substantially improved the fit between predicted and actual outcomes. The resulting models defined behavioral outcome as a function of total TBS Aβ with the following terms: y = intercept + $a \times$ [TBS Aβ] + $b \times$ [TBS Aβ]^2. This simple equation accounted for 38% of the variance in MWM total path length, 31% of variance in MWM spatial recall accuracy, and 47% of variance in RAWM working memory errors (Fig. 7, A–D; and Table S1). These models predict that a relatively small fraction of highly soluble Aβ explains an unexpectedly large proportion of the variation in cognitive performance between animals.

We then returned to the mice to ask whether the situation in vivo supported the emphasis placed on soluble Aβ by our theoretical models. Based on our models, we expected that the subtle improvement in behavioral performance between dox and dox + Ab9 mice arose in large part from a reduction of free Aβ in the brain. We used in vivo microdialysis to measure exchangeable Aβ in the interstitial fluid from a subset of dox and dox + Ab9 mice after they completed behavioral testing. A microdialysis probe with a 1 MDa cutoff size was chosen to capture all soluble Aβ species from monomeric peptide to large oligomers. Interstitial Aβ concentrations were 39% ($A\beta_{40}$) and 37% ($A\beta_{42}$) lower in mice given dox + Ab9 than in mice treated with dox alone (Fig. 7 E and Table S1), suggesting that combination treatment provided better in vivo control over behaviorally relevant forms of Aβ than APP suppression alone.

Discussion

We set out to test whether combining multiple complementary methods for Aβ reduction would improve cognitive function in amyloid-bearing transgenic mice compared with individual treatments alone. We demonstrate that combining passive anti-Aβ immunization with chemogenetic arrest of new Aβ production restored the cognitive performance of mice with severe amyloid to that of healthy age-matched controls. Computational modeling corroborated by in vivo microdialysis indicates that the combined treatment exerted its primary effect through reduction of soluble/exchangeable Aβ species. Consistent with this conclusion, thioflavin-positive fibrillar amyloid was unchanged from pretreatment, yet behavioral performance was consistently better after dox + Ab9. This outcome suggests that the mouse brain can tolerate the continued presence of fibrillar plaque cores while reestablishing effective circuits for learning and memory, provided the soluble peptide load is sufficiently reduced. Effective targeting of soluble Aβ was accompanied by attenuation of mTOR hyperactivity and, with it, a potential mechanistic link to the recovery of synaptic markers and resolution of neuritic swellings supporting functional improvement.

Although prior work had suggested the involvement of mTOR dysregulation in AD, we did not expect to find mTORC2 activity elevated by eightfold in APP/TTA mice before treatment. mTORC1 activity was less markedly elevated than mTORC2, but both were restored to control levels in mice treated with dox + Ab9. mTOR is a pleiotropic signaling protein, and its impact on diverse downstream targets could contribute to multiple pathological phenotypes in APP/TTA mice. Normal mTOR function is critical for several forms of synaptic plasticity as well as spatial and contextual memory (Costa-Mattioli and Monteggia, 2013; Bockaert and Marin, 2015). Genetic elevation of mTOR activity in mouse models of tuberous sclerosis was sufficient to impair spatial learning and contextual discrimination while lowering the threshold for synaptic potentiation; in turn, pharmacologic intervention with rapamycin rescued cognitive behavior and synaptic sensitivity, suggesting that mTOR hyperactivity was also necessary for these phenotypes (Ehninger et al., 2008). Elevated mTOR signaling has been observed in AD and Down syndrome as well as in APP/tau transgenic models and Aβ-treated primary neurons, where genetic reduction of mTOR or its downstream targets—or pharmacologic intervention with rapamycin—attenuated synaptotoxicity, restored synaptic protein markers, and rescued cognitive impairment pointing toward a causal role in these features of disease (Oddo, 2012; Talboom et al., 2015; Di Domenico et al., 2018). Beyond the synapse, mTOR signaling governs basic cellular homeostasis and negatively regulates autophagy (Saxton and Sabatini, 2017). Consistent with this role, hyperactive mTOR signaling was shown to cause autophagic arrest in models of AD and other proteinopathies where genetic or pharmacologic mTOR suppression restored autophagic flux and promoted degradation of intraneuronal aggregates (Berger et al., 2006; Crews et al., 2010; Roscic et al., 2011; Caccamo et al., 2013). Based on this evidence, we predict that the broad rescue of synaptic markers, cognitive function, and cellular homeostasis afforded by dox + Ab9 treatment here was mediated in large part by its effect on mTOR signaling. This hypothesis would be ideally tested by inducible CNS-specific mTOR knockdown, but might be more quickly, if less cleanly, examined with chronic rapamycin treatment in future experiments.

The dataset generated here allowed us to test whether and how behavioral performance in our mice depended on brain Aβ concentration. We uncovered three key findings from these analyses. First, we found that cortical Aβ levels had a strong and significant influence on performance in the two spatial navigation tasks, MWM and RAWM, but no impact on associative memory of contextual information in FC. This discrepancy may be explained by greater reliance on brain areas such as the amygdala in FC that were not tested for Aβ (Maren et al., 2013; Herry and Johansen, 2014) or may indicate that performance in this task is not dependent on Aβ load. Despite the lack of correlation between cortical Aβ and FC performance, combination treatment nevertheless produced significant improvement in this task, as it had for MWM and RAWM. The second key finding from the statistical modeling was the importance of soluble Aβ in governing performance on spatial tests of cognitive function. Past work had shown that exogenous application of oligomeric Aβ impaired synaptic plasticity and spatial learning in wild-type rodents (Walsh et al., 2002; Cleary et al., 2005; Shankar et al., 2008). Conversely, passive immunization with anti-oligomer antibody was sufficient for cognitive protection in 3xTg-AD mice (Rasool et al., 2013), whereas the efficacy of broad-spectrum IV immunoglobulin depended on its reduction of oligomeric Aβ in Dutch APP mice (Knight et al., 2016). Of note, a subset of Dutch APP mice developed cognitive deficits in the absence of deposited plaques, supporting the idea that soluble Aβ species are sufficient for functional impairment. Indeed, the presence or absence of oligomeric Aβ was sufficient to explain the observed bimodal distribution in MWM days to criteria in this model (Gandy et al., 2010). Here we build on that approach, applying multivariate statistical modeling of Aβ solubility, species, and concentration to explain individual variation in behavioral performance. This analysis confirmed prior work suggesting that the small amount of mobile Aβ in soluble form has a disproportionate influence on cognitive performance compared with the much larger concentration of Aβ held in fibrillar plaques (Dodart et al., 2002; Zhang et al., 2011; Fowler et al., 2014; Liu et al., 2015). Thus, although lowering plaque burden is a quantifiable therapeutic goal, the commensurate reduction of soluble peptide may actually have greater impact on neural function. Finally, the third important outcome of our statistical modeling was the discovery that the relationship between soluble Aβ and spatial cognition was nonlinear. This nonlinearity may reflect a biological mechanism such as receptor saturation at high Aβ concentration, or may simply arise from limits on the range of our behavioral assays. We consider both explanations likely, but suspect the limits of our assays and the behavioral range of mice in general had a bigger hand in shaping this result. Performance was more tightly defined by this relationship at low concentrations and became more variable as soluble Aβ increased.

Although straightforward in concept, testing combination anti-Aβ strategies in mice requires several approximations in practice to overcome known limitations of the available inhibitors and the animal models. One technical issue we faced with our APP/TTA transgenic model was the inability to use commercial secretase inhibitors that would have more closely approximated a multidrug regimen for clinical use. Existing γ-secretase inhibitors such as DAPT (Dovey et al., 2001), LY411575 (Wong et al., 2004), or LY450139/semagacestat (Siemers et al., 2005) are poorly tolerated for chronic use because of their side-effect profile (Imbimbo and Giardina, 2011; Golde et al., 2013; De Strooper and Chávez Gutiérrez, 2015), whereas β secretase inhibitors such as LY2811376 (May et al., 2011) are ineffective at normal dosage against transgenic APP encoding the Swedish mutation (unpublished data). We instead took advantage of the tet-transactivator system to lower Aβ production by arresting expression of transgenic APP. This genetic approach comes with its own caveats. APP overexpression can have behavioral or biochemical effects beyond those resulting from Aβ, raising the possibility that improvements seen with treatment were caused simply by suppressing these artifacts. We cannot eliminate this possibility; however, several lines of evidence mitigate its likelihood. First, the temporal dynamics of APP suppression and behavioral/biochemical recovery were markedly different. Maximal transgene suppression was attained within 4 d of

dox onset, yet cognitive function was still impaired after 2-wk dox treatment and remained statistically unchanged from pretreatment after 12 wk on dox. Second, the extent of behavioral recovery attained by dox treatment in APP/TTA mice was markedly different at 9 mo than it had been at 6 mo (Fowler et al., 2014), despite equal transgene suppression at both ages. When dox was initiated after 6 mo of APP overexpression, performance in all three tasks was restored to the level of healthy controls within 2–5 wk of treatment. When treatment was started at 9 mo here, only total errors in RAWM met this standard and only after 9–12 wk on dox. The difference in cognitive recovery observed at 6 and 9 mo may be explained by a difference in the extent of tissue damage present before treatment, but this damage is more likely caused by the rising Aβ burden than ongoing exposure to a steady concentration of other APP fragments.

The transgenic system we used to model chronic suppression of Aβ release may also underlie the pronounced difference in effect size between the individual treatments tested here. We suspect that the substantial amount of Aβ continuously produced in the APP/TTA model simply overwhelmed the binding capacity of anti-Aβ antibody. This mouse model overexpresses transgenic APP at levels ∼10-fold higher than the endogenous protein and incorporates the Swedish mutation to increase processing through the β-secretase pathway (Jankowsky et al., 2005; Rodgers et al., 2012). Transgene suppression with dox treatment thus interrupts a large pipeline of Aβ release with >95% efficacy. In contrast to dox treatment, which controls Aβ at the level of production synthesis, anti-Aβ antibody sequesters Aβ after it is released, capturing at most two peptides for every molecule of antibody. The efficacy of Ab9 is limited by three additional factors that do not affect dox treatment. First, very little antibody actually reaches the brain where most Aβ resides. The steady-state level of peripherally administered antibody within the CNS is estimated to be less than 0.1% of the total dose (Bard et al., 2000; Levites et al., 2006b; Golde et al., 2009). Second, once free antibody encounters Aβ, the resulting antigen–antibody complex is quite stable, essentially rendering the bound antibody inactive (DeMattos et al., 2001; Levites et al., 2006b). Finally, Ab9 recognizes an epitope that Aβ shares with APP (Levites et al., 2006a), diverting antibody that does reach the brain from engaging peptide. In principle, some of these limitations might have been overcome by increasing the dose of Ab9; however, at 500 µg/wk, the mice were already at the limit of what has been used in past animal studies (Hartman et al., 2005; Levites et al., 2006a) and equivalent to high-dose anti-Aβ antibody in current human clinical trials (i.e., 1,200 mg gantenerumab/∼125-lb subject ≅ 20 µg/g, for a 25 g/mouse = 500 µg). That this dose of anti-Aβ antibody which had little effect alone was sufficient to improve all outcomes when used in conjunction with Aβ suppression is particularly encouraging given the likelihood that few secretase inhibitors will lower Aβ production to the same degree as dox-mediated transgene suppression.

We hope that this study will prompt serious consideration of multidrug trials for Aβ reduction in AD. Our results indicate the reduction of soluble/exchangeable Aβ as a critical factor in cognitive efficacy and suggest that the removal of deposited peptide is beneficial only inasmuch as it eliminates a vast supply of loosely associated Aβ in exchange with the surrounding extracellular fluid. Whether mTOR mitigation is a marker or mechanism of the intracellular recuperation effected by combination therapy remains to be proven; nevertheless, it offers a provocative but testable candidate for future multidrug cocktails in animal models of AD.

Materials and methods

Mice

Mice expressing transgenic $APP^{swe/ind}$ under control of the tTA promoter (tetO-APPswe/ind line 102; Jankowsky et al., 2005) were mated to mice expressing tTA under control of the CaMKIIα promoter for these studies (CaMKIIα-tTA line B; 3010; Jackson Laboratory; Mayford et al., 1996). Each line had been independently backcrossed to C57BL/6J for >25 generations before being intercrossed. APP/TTA double transgenic B6 males were subsequently mated with wild-type FVB females to produce experimental F1 cohorts. Both male and female animals were used for experiments, balanced across treatment groups. All experiments involving live mice were reviewed and approved by the Institutional Animal Care and Use Committee of Washington University School of Medicine (in vivo microdialysis) or Baylor College of Medicine (all other experiments).

Dox administration

All mice used in this study were reared on dox from shortly after birth until postnatal day 42 (P42) to suppress APP transgene expression during postnatal development (Rodgers et al., 2012). Offspring were started on dox 1–3 d after birth by placing nursing mothers on medicated chow (100 mg/kg dox in Purina 5058 chow; F6712; BioServe). After weaning at P21, mice were maintained on dox until P42 (100 mg/kg dox in Purina 5001 chow; F6619; BioServe). At P42, mice were switched to standard Purina 5001 chow and remained on this diet until 10.5 mo of age, when animals were divided into treatment groups before behavioral testing. At that time, two groups were returned to dox chow (dox, dox + Ab9; F6619); other groups remained on standard diet.

Short-term APP suppression

To test the reversibility of cognitive deficits after short-term APP suppression, one cohort of 10.5-mo-old APP/TTA mice (allowing 9 mo of transgenic APP expression, as described above) was treated with dox chow (F6619) for 2 wk before behavioral testing and was maintained on dox until harvest.

Antibody injections

1 wk after starting on dox chow, mice received the first of 12 weekly i.p. injections containing either 500 µg purified anti-$Aβ_{1-16}$ monoclonal antibody Ab9 (Levites et al., 2006a; Wang et al., 2011) diluted in DMEM–high glucose + 10% chemically defined medium for high-density cell culture or vehicle (0.9% saline).

Behavioral assays

Behavioral testing began at 10.5 (pretreatment), 11 (acute dox suppression), or 13 mo of age (vehicle, Ab9, dox, and dox + Ab9), after at least 9 mo of transgenic APP expression in the APP/TTA animals

(or longer for vehicle and Ab9 groups). The behavioral battery is described in detail in Fowler et al., 2014. Animals were handled for 3 d before the start of behavioral testing. Open field assay began on day 1, followed by MWM training on days 2–12, RAWM training on day 13, and visible cue testing on day 14. Animals underwent FC training on day 16, with a context test 24 h later. Because the behavioral experiments spanned ∼150 mice, testing was separated into 13 experimental cohorts (∼12 animals per cohort). This group size ensured that the intertrial interval during training was similar for every animal. Each cohort included mice from all five treatment groups and at least one of two TTA controls. All animal experiments were reviewed and approved by the Baylor College of Medicine Institutional Care and Use Committee.

Visible cue testing

Although included in our earlier behavioral studies of APP/TTA mice (Fowler et al., 2014), the procedure for testing visual acuity was not described in detail. After completion of RAWM testing, visible cues were removed from the walls and the escape platform and were replaced by one marked with a pole bearing black tape that protruded 10 cm from the water surface. The platform was moved in random order between the four quadrant locations, and animals were placed into the pool directly opposite the platform for each trial. Animals were given 60 s to locate the platform and returned to their home age for 15 min between trials. Animals had to remain on the platform for at least 5 s to count as a successful trial, and were required to locate and remain on the platform for three of the four trials; animals that failed two or more trials were excluded (pretreatment, one APP/TTA; Ab9 only, two APP/TTA).

Contextual FC

Movement was recorded by a video camera counted inside the chamber and analyzed using Video Freeze software (Med Associates). Motion threshold was set to 19 arbitrary units, and the minimum freeze to 1 s. During training on the first day, mice were allowed to freely explore the chambers for 80 s before receiving a 2-s, 0.8-mA foot shock. Mice received two more 2-s, 0.8-mA foot shocks at 180 and 240 s and were returned to their home cage 60 s after the final shock. The next day, animals were returned to the conditioning chamber for a 5-min retention test. The duration of immobility was recorded and used as an index of recall.

Tissue harvest

1 d after behavioral testing ended, mice were killed by sodium pentobarbital overdose and transcardially perfused with PBS + heparin. Brains were removed and hemisected along the midline. The cortex and hippocampus of the left hemisphere were snap-frozen on dry ice and stored at −80°C; the right hemisphere was immersion-fixed in 4% PFA at 4°C for 48 h. Brains were cryoprotected in 30% sucrose at 4°C. Tissue was sectioned at 35 µm in the sagittal plane using a freezing sliding microtome and stored in cryoprotectant at −20°C until use.

Campbell–Switzer silver stain (human and mouse)

A detailed protocol for this stain can be found at the NeuroScience Associates website: https://www.neuroscienceassociates.com/reference/papers/alzheimers-disease-pathology-silver-stain/.

Thioflavin-S histology

A 1/12 series of sections spaced at 420-µm intervals were stained for thioflavin. Sagittal 35-µm sections were rinsed, mounted onto Superfrost Plus slides, and dried overnight. Sections were rehydrated in running tap water and incubated for 10–15 min in 0.25% potassium permanganate followed by 5 min in 1% potassium metabisulfite/1% oxalic acid, before staining in 0.02% Thioflavine-S (T1892; Sigma) for 8 min. Staining was differentiated in 80% ethanol followed by running tap water. Sections were dehydrated through xylene and coverslipped with Permount.

Ubiquitin immunohistochemistry

A 1/12 series of sections were mounted onto Superfrost Plus slides and allowed to dry overnight. Slide-mounted sections were rehydrated in TBS before undergoing antigen retrieval in 10 mM sodium citrate buffer (pH 6.0) using a pressure cooker (Duo; 918060242; Fagor America). For this process, slides were placed into a metal slide tray and immersed in citrate buffer inside the cooker. Once closed, the cooker was set on high (15 psi) and heated on a Bunsen burner until the pressure indicator tripped. The cooker was allowed to heat for an additional 10 min on the burner, then was removed from heat and cooled to room temperature before opening (accelerated by placing the unit into ice water). Slides were then removed from the citrate buffer, rinsed in TBS, and immersed in TBS containing 0.1% Triton X-100 (TBST) plus 0.9% H_2O_2 for 15 min at room temperature to inactivate endogenous peroxidases. After peroxidase treatment, nonspecific binding was blocked for 1 h at room temperature with TBS containing 5% normal horse serum before overnight incubation at 4°C with mouse anti-ubiquitin antibody (ab7254; Abcam) diluted 1:500 in blocking solution. After several washes in TBS, slides were incubated for 2 h at room temperature with biotin-conjugated horse anti-mouse secondary antibody (PK-6102; Vectastain Elite ABC, Mouse IgG; Vector Laboratories) diluted 1:500 in blocking solution. Slides were then washed in TBS, followed by 30 min at room temperature in HRP-avidin conjugate diluted 1:50 in TBS. Sections were developed with diaminobenzidine (D4418; Sigma), dehydrated, and coverslipped with Permount.

Immunofluorescence (NAB61, synaptophysin, PSD95, LAMP1, TFEB, and REEP5)

A 1/12 series of sections were rinsed with TBS and blocked with TBST containing 10% normal goat serum for 1 h at room temperature before overnight incubation at 4°C with mouse anti-Aβ antibody NAB61 (gift of V. Lee, University of Pennsylvania, Philadelphia, PA), rabbit anti-synaptophysin (AB9272; Millipore), rabbit anti-PSD95 (ab18258; Abcam), mouse anti-LAMP1 (1D4B; Developmental Studies Hybridoma Bank), rabbit anti-TFEB (1:1,000; A303-673A; Bethyl Laboratories), or rabbit anti-REEP5 (14643-1-AP; Protein Tech), each diluted 1:500 in blocking solution. After several washes in TBS, sections were incubated with Alexa Fluor 568–conjugated secondary antibody (A11004 for goat anti–mouse; A11036 for goat anti–rabbit; Invitrogen) diluted 1:500 in block for 2 h at room temperature. Sections were washed with TBS before being counterstained for 8 min at room temperature with 0.002% thioflavin-S diluted in TBS. After two 1-min washes in 50% ethanol followed by several washes in TBS, sections were

mounted on Superfrost Plus slides and coverslipped with Vectashield mounting medium (H1400; Vector Laboratories).

Quantification of amyloid burden, synapse area, and dystrophic neurites

All imaging was performed with an Axio Imager Z1 microscope (Zeiss) using Zen 2012 software v.1.1.2.0. Bright-field and immunofluorescent image mosaics were acquired by sequential scanning with a motorized stage, stitched, and exported as tiff files. Sections stained for Campbell–Switzer silver, NAB61, thioflavin-S, ubiquitin, and LAMP1 were quantified in Matlab (v.8.6 R2015b; MathWorks). Automated color thresholds were used to distinguish signal from background across the entire stained section and quantified as a percentage of area within a manually outlined region of interest (cortex or hippocampus). Four to five sections spaced at 420-µm intervals were measured for each animal. The Matlab code for this analysis is publicly available for download on the Matlab File Exchange (https://www.mathworks.com/matlabcentral/fileexchange/63987-percent-area-roi).

Quantification of synapse area

For synaptophysin analysis, four nonoverlapping 40× fields centered on an isolated plaque were imaged from each of four tissue sections for each animal (16 fields per animal). A single optical plane was collected for each field in the red (synaptophysin) and green (thioflavin-S) channels using an Apotome structured illumination device (Zeiss). A custom Matlab script was written for analysis. Each color channel was first converted to binary signal. The thioflavin image was used to outline the plaque using binary boundary detection. The code then dilated this boundary by 10, 20, and 30 µm and applied the outlines onto the thresholded red channel to compute the area of synaptophysin signal as a percentage of total area in each annulus. The Matlab code for this analysis is publicly available for download on the Matlab File Exchange (https://www.mathworks.com/matlabcentral/fileexchange/63971-synaptophysinroidilation).

Immunoblotting

Frozen brain samples were prepared for Western blotting by sonication in five volumes of PBS containing 1× protease and phosphatase inhibitors (5892970001 and 04906845001; Sigma) then diluted with an equal volume of 2× concentrated RIPA buffer (1× PBS + 2% SDS + 1% NP-40 + 1% deoxycholate + 5 mM EDTA) and centrifuged at 16,100 *g* for 10 min at 4°C. For most immunoblots, 10 µl supernatant was mixed with an equal volume of 2× Laemmli buffer and denatured at 95°C for 5 min before being loaded onto 4–15% Tris-HCl gels (3450028; Bio-Rad). After electrophoresis, proteins were transferred to nitrocellulose membrane (Trans-Blot Turbo Transfer kit 1704271; Bio-Rad), blocked in PBS containing 0.1% Tween-20 (PBSTw) and 5% nonfat dry milk for 1 h at room temperature, and probed overnight at 4° with one or more of the following primary antibodies: 6E10 (1:5,000; 803001; BioLegend), TFEB (1:1,000; A303-673A; Bethyl Laboratories), p-$s6_{s244/240}$ ribosomal protein (1:2,000; 5364; Cell Signaling Technology), and p-AKT_{s473} (1:2,000; 4060; Cell Signaling Technology), p-cofilin (1:1,000; 3311; Cell Signaling Technology), or GAPDH (1:5,000; AB2302; Millipore). Blots were washed several times with PBSTw, incubated for 3 h at room temperature with IRDye-conjugated secondary antibodies (926-32212, 926-32214, 926-32213, or 926-68075, each diluted 1:10,000; LI-COR Biosciences), and imaged with an Odyssey Fc detection system. After imaging, blots for p-s6 ribosomal protein and p-AKT were stripped (928-40030; LI-COR Biosciences), reblocked, and reprobed for total s6 ribosomal protein (1:1,000; 2217; Cell Signaling Technology), total AKT (1:1,000; 4691; Cell Signaling Technology), or total cofilin (1:1,000; 5175; Cell Signaling Technology). Densitometry analyses were performed using Image Studio Lite software v.5.2 (LI-COR Biosciences).

ELISA

Frozen cortical samples were prepared for Aβ ELISA by sequential biochemical extraction as described previously (Youmans et al., 2011). Cortical tissue from one hemisphere was sonicated in cold TBS containing 1× protease and phosphatase inhibitors (5892970001 and 04906845001; Sigma) at a ratio of 1 ml per 150 mg tissue weight. The homogenate was centrifuged at 100,000 *g* for 1 h at 4°C, and the supernatant was collected as TBS-soluble extract. The pellet was resuspended to its original volume by pipetting in TBS containing protease and phosphatase inhibitor + 1% Triton X-100 (TBSX) and mixed by gentle rotation at 4°C for 30 min. The homogenate was centrifuged at 100,000 *g* for 1 h at 4°C, and the supernatant was collected as TBSX-soluble extract. The TBSX pellet was resuspended to its original volume by pipetting in 50 mM Tris-HCl, pH 6.8, containing 5 M guanidine hydrochloride and mixed by gentle rotation at room temperature overnight. The next day, samples were centrifuged at 16,000 *g* for 30 min at room temperature, and the supernatant was collected as the guanidine-soluble extract. All samples were stored at −80°C until use. Aβ levels were determined by end-specific sandwich ELISAs using monoclonal antibody 2.1.3 (human Aβx-42 specific) and 13.1.1 (human Aβx-40 specific) for capture, and HRP-conjugated monoclonal antibody Ab5 (human Aβ1-16 specific) for detection, modified from an earlier assay (Chakrabarty et al., 2015).

Microdialysis

Microdialysis was performed as described previously (Cirrito et al., 2003; Ulrich et al., 2013) using a 1-MDa molecular weight cutoff microdialysis probe. In brief, dox- and dox + Ab9–treated mice were continued on their respective therapies after completion of behavioral testing. The microdialysis guide cannula were stereotaxically implanted with the guide cannula tip (Eicom) at coordinates bregma −3.1 mm, 2.5 mm from midline 1.2 mm below the dura at a 12° angle. After surgery, mice recovered for 24 h followed by insertion of a 1-MDa molecular weight cutoff microdialysis probe that was 2 mm in length (AtmosLM probe; Eicom). Mice had freedom of movement and ad libitum food and water. Artificial CSF containing 0.15% BSA was perfused through the microdialysis probe at a constant flow rate (inward rate, 1.1 µl/min; outward rate, 1.0 µl/min). Microdialysis samples were collected every 60–180 min in a refrigerated fraction collector. After the final collection, samples were assayed for Aβx-40 and Aβx-42 by sandwich ELISA using mouse anti-Aβ antibodies mHJ2 or mHJ7.4 for capture, respectively, and biotinylated mHJ5.1 for detection (Fisher et al., 2016).

Statistical analysis

Data were analyzed using one- or two-way ANOVA or *t* test where appropriate for values with approximately normal distribution. All ANOVA post hoc comparisons were conducted using Tukey testing. Datasets characterized by a nonnormal distribution were analyzed using Kruskal–Wallis testing followed by Dunn's post hoc comparisons. Most statistical analyses and all graphs were created using Prism 6.0 (GraphPad). Bar graphs display group means ± SEM. Multivariate ANOVA analysis was performed in SPSS v.23. Correlation analysis and general linear modeling were performed using R (v.3.3.3; R Core Team, 2017) packages: effects (v.3.1.2; Fox, 2003), MASS (v.7.3.45; Venables and Ripley, 2002), RCMDR (v.2.3.2; Fox and Bouchet-Valat, 2017), sandwich (v.2.3.4; Zeileis, 2004), and car (v.2.1.4; Fox and Weisberg, 2011).

Online supplemental material

Fig. S1 shows that acute suppression of Aβ overproduction fails to reverse cognitive impairments in aged APP/TTA mice. Fig. S2 shows histological analysis of plaque burden in the hippocampus. Fig. S3 shows biochemical measurements of Aβ40, Aβ42, and total Aβ levels measured by ELISA for each treatment group. Fig. S4 shows additional control experiments from behavioral testing. Table S1 provides detailed statistical outcomes for all quantitative comparisons performed in these experiments.

Acknowledgments

We thank Rebecca Corrigan for animal care, Kurt Christensen and Dean Edwards of the Baylor College of Medicine Monoclonal Antibody/Recombinant Protein Expression Core for monoclonal services, Todd Golde and Thomas Ladd for characterizing the monoclonal preparation, Virginia Lee for the gift of NAB61 antibody, Kira Chen for graphical abstract artwork, and members of the Jankowsky laboratory for helpful discussion.

This work was supported by National Institutes of Health grant R01 NS092515 and a gift from the Robert A. and Rene E. Belfer Family Foundation (J.L. Jankowsky). A.C.A. Chiang was supported by National Institutes of Health Biology of Aging training grant T32 AG000183 and a Gates Millennium Scholarship. The Monoclonal Antibody/Recombinant Protein Expression Shared Resource at Baylor College of Medicine was funded by National Institutes of Health Cancer Center Support Grant P30 CA125123.

The authors declare no competing financial interests.

Author contributions: A.C.A. Chiang and J.L. Jankowsky designed the experiments and wrote the paper; A.C.A. Chiang performed animal treatments, histology, immunostaining, Western blotting, and quantitative analyses; A.C.A. Chiang and S.W. Fowler performed mouse behavioral testing; R.R. Savjani wrote the Matlab code used for image analysis, S.G. Hilsenbeck performed statistical modeling, C.E. Wallace and J.R. Cirrito performed in vivo microdialysis; and P. Das performed ELISA assays.

Submitted: 14 August 2017
Revised: 3 January 2018
Accepted: 7 March 2018

References

Alamed, J., D.M. Wilcock, D.M. Diamond, M.N. Gordon, and D. Morgan. 2006. Two-day radial-arm water maze learning and memory task; robust resolution of amyloid-related memory deficits in transgenic mice. *Nat. Protoc.* 1:1671–1679. https://doi.org/10.1038/nprot.2006.275

An, W.L., R.F. Cowburn, L. Li, H. Braak, I. Alafuzoff, K. Iqbal, I.G. Iqbal, B. Winblad, and J.J. Pei. 2003. Up-regulation of phosphorylated/activated p70 S6 kinase and its relationship to neurofibrillary pathology in Alzheimer's disease. *Am. J. Pathol.* 163:591–607. https://doi.org/10.1016/S0002-9440(10)63687-5

Bard, F., C. Cannon, R. Barbour, R.L. Burke, D. Games, H. Grajeda, T. Guido, K. Hu, J. Huang, K. Johnson-Wood, et al. 2000. Peripherally administered antibodies against amyloid beta-peptide enter the central nervous system and reduce pathology in a mouse model of Alzheimer disease. *Nat. Med.* 6:916–919. https://doi.org/10.1038/78682

Bayat Mokhtari, R., T.S. Homayouni, N. Baluch, E. Morgatskaya, S. Kumar, B. Das, and H. Yeger. 2017. Combination therapy in combating cancer. *Oncotarget.* 8:38022–38043.

Berger, Z., B. Ravikumar, F.M. Menzies, L.G. Oroz, B.R. Underwood, M.N. Pangalos, I. Schmitt, U. Wullner, B.O. Evert, C.J. O'Kane, and D.C. Rubinsztein. 2006. Rapamycin alleviates toxicity of different aggregate-prone proteins. *Hum. Mol. Genet.* 15:433–442. https://doi.org/10.1093/hmg/ddi458

Bockaert, J., and P. Marin. 2015. mTOR in brain physiology and pathologies. *Physiol. Rev.* 95:1157–1187. https://doi.org/10.1152/physrev.00038.2014

Caccamo, A., S. Majumder, A. Richardson, R. Strong, and S. Oddo. 2010. Molecular interplay between mammalian target of rapamycin (mTOR), amyloid-beta, and Tau: Effects on cognitive impairments. *J. Biol. Chem.* 285:13107–13120. https://doi.org/10.1074/jbc.M110.100420

Caccamo, A., M.A. Maldonado, S. Majumder, D.X. Medina, W. Holbein, A. Magrí, and S. Oddo. 2011. Naturally secreted amyloid-beta increases mammalian target of rapamycin (mTOR) activity via a PRAS40-mediated mechanism. *J. Biol. Chem.* 286:8924–8932. https://doi.org/10.1074/jbc.M110.180638

Caccamo, A., A. Magrì, D.X. Medina, E.V. Wisely, M.F. López-Aranda, A.J. Silva, and S. Oddo. 2013. mTOR regulates tau phosphorylation and degradation: Implications for Alzheimer's disease and other tauopathies. *Aging Cell.* 12:370–380. https://doi.org/10.1111/acel.12057

Calabrese, B., G.M. Shaked, I.V. Tabarean, J. Braga, E.H. Koo, and S. Halpain. 2007. Rapid, concurrent alterations in pre- and postsynaptic structure induced by naturally-secreted amyloid-beta protein. *Mol. Cell. Neurosci.* 35:183–193. https://doi.org/10.1016/j.mcn.2007.02.006

Chakrabarty, P., A. Li, C. Ceballos-Diaz, J.A. Eddy, C.C. Funk, B. Moore, N. DiNunno, A.M. Rosario, P.E. Cruz, C. Verbeeck, et al. 2015. IL-10 alters immunoproteostasis in APP mice, increasing plaque burden and worsening cognitive behavior. *Neuron.* 85:519–533. https://doi.org/10.1016/j.neuron.2014.11.020

Chiang, A.C.A., S.W. Fowler, R. Reddy, O. Pletnikova, J.C. Troncoso, M.A. Sherman, S.E. Lesne, and J.L. Jankowsky. 2018. Discrete pools of oligomeric amyloid-beta track with spatial learning deficits in a mouse model of Alzheimer amyloidosis. *Am. J. Pathol.* 188:739–756.

Chiang, A.C.A., S.W. Fowler, R. Reddy, O. Pletnikova, J.C. Troncoso, M.A. Sherman, S.E. Lesne, and J.L. Jankowsky. 2018. Discrete pools of oligomeric amyloid-β track with spatial learning deficits in a mouse model of Alzheimer amyloidosis. *Am. J. Pathol.* 188:739–756. https://doi.org/10.1016/j.ajpath.2017.11.011

Chow, V.W., A.V. Savonenko, T. Melnikova, H. Kim, D.L. Price, T. Li, and P.C. Wong. 2010. Modeling an anti-amyloid combination therapy for Alzheimer's disease. *Sci. Transl. Med.* 2:13ra1. https://doi.org/10.1126/scitranslmed.3000337

Cirrito, J.R., P.C. May, M.A. O'Dell, J.W. Taylor, M. Parsadanian, J.W. Cramer, J.E. Audia, J.S. Nissen, K.R. Bales, S.M. Paul, et al. 2003. In vivo assessment of brain interstitial fluid with microdialysis reveals plaque-associated changes in amyloid-beta metabolism and half-life. *J. Neurosci.* 23:8844–8853.

Cleary, J.P., D.M. Walsh, J.J. Hofmeister, G.M. Shankar, M.A. Kuskowski, D.J. Selkoe, and K.H. Ashe. 2005. Natural oligomers of the amyloid-beta protein specifically disrupt cognitive function. *Nat. Neurosci.* 8:79–84. https://doi.org/10.1038/nn1372

Condello, C., A. Schain, and J. Grutzendler. 2011. Multicolor time-stamp reveals the dynamics and toxicity of amyloid deposition. *Sci. Rep.* 1:19. https://doi.org/10.1038/srep00019

Condello, C., P. Yuan, A. Schain, and J. Grutzendler. 2015. Microglia constitute a barrier that prevents neurotoxic protofibrillar Aβ42 hotspots around plaques. *Nat. Commun.* 6:6176. https://doi.org/10.1038/ncomms7176

Costa-Mattioli, M., and L.M. Monteggia. 2013. mTOR complexes in neurodevelopmental and neuropsychiatric disorders. *Nat. Neurosci.* 16:1537–1543. https://doi.org/10.1038/nn.3546

Crews, L., B. Spencer, P. Desplats, C. Patrick, A. Paulino, E. Rockenstein, L. Hansen, A. Adame, D. Galasko, and E. Masliah. 2010. Selective molecular alterations in the autophagy pathway in patients with Lewy body disease and in models of alpha-synucleinopathy. *PLoS One.* 5:e9313. https://doi.org/10.1371/journal.pone.0009313

DeMattos, R.B., K.R. Bales, D.J. Cummins, J.C. Dodart, S.M. Paul, and D.M. Holtzman. 2001. Peripheral anti-A beta antibody alters CNS and plasma A beta clearance and decreases brain A beta burden in a mouse model of Alzheimer's disease. *Proc. Natl. Acad. Sci. USA.* 98:8850–8855. https://doi.org/10.1073/pnas.151261398

De Strooper, B., and L. Chávez Gutiérrez. 2015. Learning by failing: Ideas and concepts to tackle γ-secretases in Alzheimer's disease and beyond. *Annu. Rev. Pharmacol. Toxicol.* 55:419–437. https://doi.org/10.1146/annurev-pharmtox-010814-124309

Devi, L., and M. Ohno. 2015. A combination Alzheimer's therapy targeting BACE1 and neprilysin in 5XFAD transgenic mice. *Mol. Brain.* 8:19. https://doi.org/10.1186/s13041-015-0110-5

Dickson, D.W., A. Wertkin, L.A. Mattiace, E. Fier, Y. Kress, P. Davies, and S.H. Yen. 1990. Ubiquitin immunoelectron microscopy of dystrophic neurites in cerebellar senile plaques of Alzheimer's disease. *Acta Neuropathol.* 79:486–493. https://doi.org/10.1007/BF00296107

Di Domenico, F., A. Tramutola, C. Foppoli, E. Head, M. Perluigi, and D.A. Butterfield. 2018. mTOR in Down syndrome: Role in Aß and tau neuropathology and transition to Alzheimer disease-like dementia. *Free Radic. Biol. Med.* 114:94–101. https://doi.org/10.1016/j.freeradbiomed.2017.08.009

Dodart, J.C., K.R. Bales, K.S. Gannon, S.J. Greene, R.B. DeMattos, C. Mathis, C.A. DeLong, S. Wu, X. Wu, D.M. Holtzman, and S.M. Paul. 2002. Immunization reverses memory deficits without reducing brain Abeta burden in Alzheimer's disease model. *Nat. Neurosci.* 5:452–457. https://doi.org/10.1038/nn842

Dong, H., M.V. Martin, S. Chambers, and J.G. Csernansky. 2007. Spatial relationship between synapse loss and beta-amyloid deposition in Tg2576 mice. *J. Comp. Neurol.* 500:311–321. https://doi.org/10.1002/cne.21176

Dorostkar, M.M., S. Burgold, S. Filser, S. Barghorn, B. Schmidt, U.R. Anumala, H. Hillen, C. Klein, and J. Herms. 2014. Immunotherapy alleviates amyloid-associated synaptic pathology in an Alzheimer's disease mouse model. *Brain.* 137:3319–3326. https://doi.org/10.1093/brain/awu280

Dovey, H.F., V. John, J.P. Anderson, L.Z. Chen, P. de Saint Andrieu, L.Y. Fang, S.B. Freedman, B. Folmer, E. Goldbach, E.J. Holsztynska, et al. 2001. Functional gamma-secretase inhibitors reduce beta-amyloid peptide levels in brain. *J. Neurochem.* 76:173–181. https://doi.org/10.1046/j.1471-4159.2001.00012.x

Ehninger, D., S. Han, C. Shilyansky, Y. Zhou, W. Li, D.J. Kwiatkowski, V. Ramesh, and A.J. Silva. 2008. Reversal of learning deficits in a Tsc2+/- mouse model of tuberous sclerosis. *Nat. Med.* 14:843–848. https://doi.org/10.1038/nm1788

Fisher, J.R., C.E. Wallace, D.L. Tripoli, Y.I. Sheline, and J.R. Cirrito. 2016. Redundant Gs-coupled serotonin receptors regulate amyloid-β metabolism in vivo. *Mol. Neurodegener.* 11:45. https://doi.org/10.1186/s13024-016-0112-5

Fowler, S.W., A.C. Chiang, R.R. Savjani, M.E. Larson, M.A. Sherman, D.R. Schuler, J.R. Cirrito, S.E. Lesné, and J.L. Jankowsky. 2014. Genetic modulation of soluble Aβ rescues cognitive and synaptic impairment in a mouse model of Alzheimer's disease. *J. Neurosci.* 34:7871–7885. https://doi.org/10.1523/JNEUROSCI.0572-14.2014

Fox, J. 2003. Effect displays in R for generalised linear models. *J. Stat. Softw.* 8:1–27. https://doi.org/10.18637/jss.v008.i15

Fox, J., and M. Bouchet-Valat. 2017. Rcmdr: R Commander. http://socserv.socsci.mcmaster.ca/jfox/Misc/Rcmdr/ (accessed June 1, 2017).

Fox, J., and S. Weisberg. 2011. An R companion to applied regression. Second edition. Sage Publications, Thousand Oaks, CA. 472 pp.

Gandy, S., A.J. Simon, J.W. Steele, A.L. Lublin, J.J. Lah, L.C. Walker, A.I. Levey, G.A. Krafft, E. Levy, F. Checler, et al. 2010. Days to criterion as an indicator of toxicity associated with human Alzheimer amyloid-beta oligomers. *Ann. Neurol.* 68:220–230.

Garza-Lombó, C., and M.E. Gonsebatt. 2016. Mammalian target of rapamycin: Its role in early neural development and in adult and aged brain function. *Front. Cell. Neurosci.* 10:157. https://doi.org/10.3389/fncel.2016.00157

Golde, T.E., P. Das, and Y. Levites. 2009. Quantitative and mechanistic studies of Abeta immunotherapy. *CNS Neurol. Disord. Drug Targets.* 8:31–49. https://doi.org/10.2174/187152709787601830

Golde, T.E., E.H. Koo, K.M. Felsenstein, B.A. Osborne, and L. Miele. 2013. γ-Secretase inhibitors and modulators. *Biochim. Biophys. Acta.* 1828:2898–2907. https://doi.org/10.1016/j.bbamem.2013.06.005

Griffin, R.J., A. Moloney, M. Kelliher, J.A. Johnston, R. Ravid, P. Dockery, R. O'Connor, and C. O'Neill. 2005. Activation of Akt/PKB, increased phosphorylation of Akt substrates and loss and altered distribution of Akt and PTEN are features of Alzheimer's disease pathology. *J. Neurochem.* 93:105–117. https://doi.org/10.1111/j.1471-4159.2004.02949.x

Günthard, H.F., M.S. Saag, C.A. Benson, C. del Rio, J.J. Eron, J.E. Gallant, J.F. Hoy, M.J. Mugavero, P.E. Sax, M.A. Thompson, et al. 2016. Antiretroviral drugs for treatment and prevention of HIV infection in adults: 2016 recommendations of the International Antiviral Society-USA Panel. *JAMA.* 316:191–210. https://doi.org/10.1001/jama.2016.8900

Hartman, R.E., Y. Izumi, K.R. Bales, S.M. Paul, D.F. Wozniak, and D.M. Holtzman. 2005. Treatment with an amyloid-beta antibody ameliorates plaque load, learning deficits, and hippocampal long-term potentiation in a mouse model of Alzheimer's disease. *J. Neurosci.* 25:6213–6220. https://doi.org/10.1523/JNEUROSCI.0664-05.2005

Hendrix, J.A., R.J. Bateman, H.R. Brashear, C. Duggan, M.C. Carrillo, L.J. Bain, R. DeMattos, R.G. Katz, S. Ostrowitzki, E. Siemers, et al. 2016. Challenges, solutions, and recommendations for Alzheimer's disease combination therapy. *Alzheimers Dement.* 12:623–630. https://doi.org/10.1016/j.jalz.2016.02.007

Herry, C., and J.P. Johansen. 2014. Encoding of fear learning and memory in distributed neuronal circuits. *Nat. Neurosci.* 17:1644–1654. https://doi.org/10.1038/nn.3869

Hoeffer, C.A., and E. Klann. 2010. mTOR signaling: At the crossroads of plasticity, memory and disease. *Trends Neurosci.* 33:67–75. https://doi.org/10.1016/j.tins.2009.11.003

Huang, W., P.J. Zhu, S. Zhang, H. Zhou, L. Stoica, M. Galiano, K. Krnjević, G. Roman, and M. Costa-Mattioli. 2013. mTORC2 controls actin polymerization required for consolidation of long-term memory. *Nat. Neurosci.* 16:441–448. https://doi.org/10.1038/nn.3351

Imbimbo, B.P., and G.A. Giardina. 2011. γ-Secretase inhibitors and modulators for the treatment of Alzheimer's disease: Disappointments and hopes. *Curr. Top. Med. Chem.* 11:1555–1570. https://doi.org/10.2174/156802611795860942

Jacobsen, H., L. Ozmen, A. Caruso, R. Narquizian, H. Hilpert, B. Jacobsen, D. Terwel, A. Tanghe, and B. Bohrmann. 2014. Combined treatment with a BACE inhibitor and anti-Aβ antibody gantenerumab enhances amyloid reduction in APPLondon mice. *J. Neurosci.* 34:11621–11630. https://doi.org/10.1523/JNEUROSCI.1405-14.2014

Jankowsky, J.L., H.H. Slunt, V. Gonzales, A.V. Savonenko, J.C. Wen, N.A. Jenkins, N.G. Copeland, L.H. Younkin, H.A. Lester, S.G. Younkin, and D.R. Borchelt. 2005. Persistent amyloidosis following suppression of Abeta production in a transgenic model of Alzheimer disease. *PLoS Med.* 2:e355. https://doi.org/10.1371/journal.pmed.0020355

Kerantzas, C.A., and W.R. Jacobs Jr. 2017. Origins of combination therapy for tuberculosis: Lessons for future antimicrobial development and application. *MBio.* 8:e01586–e16. https://doi.org/10.1128/mBio.01586-16

Knight, E.M., S.H. Kim, J.C. Kottwitz, A. Hatami, R. Albay, A. Suzuki, A. Lublin, C.M. Alberini, W.L. Klein, P. Szabo, et al. 2016. Effective anti-Alzheimer Aβ therapy involves depletion of specific Aβ oligomer subtypes. *Neurol. Neuroimmunol. Neuroinflamm.* 3:e237. https://doi.org/10.1212/NXI.0000000000000237

Knowles, R.B., C. Wyart, S.V. Buldyrev, L. Cruz, B. Urbanc, M.E. Hasselmo, H.E. Stanley, and B.T. Hyman. 1999. Plaque-induced neurite abnormalities: Implications for disruption of neural networks in Alzheimer's disease. *Proc. Natl. Acad. Sci. USA.* 96:5274–5279. https://doi.org/10.1073/pnas.96.9.5274

Koffie, R.M., M. Meyer-Luehmann, T. Hashimoto, K.W. Adams, M.L. Mielke, M. Garcia-Alloza, K.D. Micheva, S.J. Smith, M.L. Kim, V.M. Lee, et al. 2009. Oligomeric amyloid beta associates with postsynaptic densities and correlates with excitatory synapse loss near senile plaques. *Proc. Natl. Acad. Sci. USA.* 106:4012–4017. https://doi.org/10.1073/pnas.0811698106

Lacor, P.N., M.C. Buniel, P.W. Furlow, A.S. Clemente, P.T. Velasco, M. Wood, K.L. Viola, and W.L. Klein. 2007. Abeta oligomer-induced aberrations in synapse composition, shape, and density provide a molecular basis for loss of connectivity in Alzheimer's disease. *J. Neurosci.* 27:796–807. https://doi.org/10.1523/JNEUROSCI.3501-06.2007

Lee, E.B., L.Z. Leng, B. Zhang, L. Kwong, J.Q. Trojanowski, T. Abel, and V.M. Lee. 2006. Targeting amyloid-beta peptide (Abeta) oligomers by passive immunization with a conformation-selective monoclonal antibody improves learning and memory in Abeta precursor protein (APP)

transgenic mice. *J. Biol. Chem.* 281:4292–4299. https://doi.org/10.1074/jbc.M511018200

Levites, Y., P. Das, R.W. Price, M.J. Rochette, L.A. Kostura, E.M. McGowan, M.P. Murphy, and T.E. Golde. 2006a. Anti-Abeta42- and anti-Abeta40-specific mAbs attenuate amyloid deposition in an Alzheimer disease mouse model. *J. Clin. Invest.* 116:193–201. https://doi.org/10.1172/JCI25410

Levites, Y., L.A. Smithson, R.W. Price, R.S. Dakin, B. Yuan, M.R. Sierks, J. Kim, E. McGowan, D.K. Reed, T.L. Rosenberry, et al. 2006b. Insights into the mechanisms of action of anti-Abeta antibodies in Alzheimer's disease mouse models. *FASEB J.* 20:2576–2578. https://doi.org/10.1096/fj.06-6463fje

Liu, P., M.N. Reed, L.A. Kotilinek, M.K. Grant, C.L. Forster, W. Qiang, S.L. Shapiro, J.H. Reichl, A.C. Chiang, J.L. Jankowsky, et al. 2015. Quaternary structure defines a large class of amyloid-β oligomers neutralized by sequestration. *Cell Reports.* 11:1760–1771. https://doi.org/10.1016/j.celrep.2015.05.021

Maren, S., K.L. Phan, and I. Liberzon. 2013. The contextual brain: Implications for fear conditioning, extinction and psychopathology. *Nat. Rev. Neurosci.* 14:417–428. https://doi.org/10.1038/nrn3492

May, P.C., R.A. Dean, S.L. Lowe, F. Martenyi, S.M. Sheehan, L.N. Boggs, S.A. Monk, B.M. Mathes, D.J. Mergott, B.M. Watson, et al. 2011. Robust central reduction of amyloid-β in humans with an orally available, non-peptidic β-secretase inhibitor. *J. Neurosci.* 31:16507–16516. https://doi.org/10.1523/JNEUROSCI.3647-11.2011

Mayford, M., M.E. Bach, Y.Y. Huang, L. Wang, R.D. Hawkins, and E.R. Kandel. 1996. Control of memory formation through regulated expression of a CaMKII transgene. *Science.* 274:1678–1683. https://doi.org/10.1126/science.274.5293.1678

Nixon, R.A. 2007. Autophagy, amyloidogenesis and Alzheimer disease. *J. Cell Sci.* 120:4081–4091. https://doi.org/10.1242/jcs.019265

Nixon, R.A., and D.S. Yang. 2011. Autophagy failure in Alzheimer's disease—Locating the primary defect. *Neurobiol. Dis.* 43:38–45. https://doi.org/10.1016/j.nbd.2011.01.021

Oddo, S. 2012. The role of mTOR signaling in Alzheimer disease. *Front. Biosci. (Schol. Ed.).* 4:941–952. https://doi.org/10.2741/s310

Perry, D., R. Sperling, R. Katz, D. Berry, D. Dilts, D. Hanna, S. Salloway, J.Q. Trojanowski, C. Bountra, M. Krams, et al. 2015. Building a roadmap for developing combination therapies for Alzheimer's disease. *Expert Rev. Neurother.* 15:327–333. https://doi.org/10.1586/14737175.2015.996551

Rasool, S., H. Martinez-Coria, J.W. Wu, F. LaFerla, and C.G. Glabe. 2013. Systemic vaccination with anti-oligomeric monoclonal antibodies improves cognitive function by reducing Aβ deposition and tau pathology in 3xTg-AD mice. *J. Neurochem.* 126:473–482. https://doi.org/10.1111/jnc.12305

R Core Team. 2017. R: A language and environment for statistical computing. R Foundation for Statistical Computing, Vienna, Austria. https://www.r-project.org/ (accessed June 1, 2017).

Rodgers, S.P., H.A. Born, P. Das, and J.L. Jankowsky. 2012. Transgenic APP expression during postnatal development causes persistent locomotor hyperactivity in the adult. *Mol. Neurodegener.* 7:28. https://doi.org/10.1186/1750-1326-7-28

Roscic, A., B. Baldo, C. Crochemore, D. Marcellin, and P. Paganetti. 2011. Induction of autophagy with catalytic mTOR inhibitors reduces huntingtin aggregates in a neuronal cell model. *J. Neurochem.* 119:398–407. https://doi.org/10.1111/j.1471-4159.2011.07435.x

Sardiello, M., M. Palmieri, A. di Ronza, D.L. Medina, M. Valenza, V.A. Gennarino, C. Di Malta, F. Donaudy, V. Embrione, R.S. Polishchuk, et al. 2009. A gene network regulating lysosomal biogenesis and function. *Science.* 325:473–477.

Saxton, R.A., and D.M. Sabatini. 2017. mTOR signaling in growth, metabolism, and disease. *Cell.* 168:960–976. https://doi.org/10.1016/j.cell.2017.02.004

Settembre, C., C. Di Malta, V.A. Polito, M. Garcia Arencibia, F. Vetrini, S. Erdin, S.U. Erdin, T. Huynh, D. Medina, P. Colella, et al. 2011. TFEB links autophagy to lysosomal biogenesis. *Science.* 332:1429–1433. https://doi.org/10.1126/science.1204592

Shankar, G.M., B.L. Bloodgood, M. Townsend, D.M. Walsh, D.J. Selkoe, and B.L. Sabatini. 2007. Natural oligomers of the Alzheimer amyloid-beta protein induce reversible synapse loss by modulating an NMDA-type glutamate receptor-dependent signaling pathway. *J. Neurosci.* 27:2866–2875. https://doi.org/10.1523/JNEUROSCI.4970-06.2007

Shankar, G.M., S. Li, T.H. Mehta, A. Garcia-Munoz, N.E. Shepardson, I. Smith, F.M. Brett, M.A. Farrell, M.J. Rowan, C.A. Lemere, et al. 2008. Amyloid-beta protein dimers isolated directly from Alzheimer's brains impair synaptic plasticity and memory. *Nat. Med.* 14:837–842. https://doi.org/10.1038/nm1782

Sharoar, M.G., Q. Shi, Y. Ge, W. He, X. Hu, G. Perry, X. Zhu, and R. Yan. 2016. Dysfunctional tubular endoplasmic reticulum constitutes a pathological feature of Alzheimer's disease. *Mol. Psychiatry.* 21:1263–1271. https://doi.org/10.1038/mp.2015.181

Siemers, E., M. Skinner, R.A. Dean, C. Gonzales, J. Satterwhite, M. Farlow, D. Ness, and P.C. May. 2005. Safety, tolerability, and changes in amyloid beta concentrations after administration of a gamma-secretase inhibitor in volunteers. *Clin. Neuropharmacol.* 28:126–132. https://doi.org/10.1097/01.wnf.0000167360.27670.29

Stephenson, D., D. Perry, C. Bens, L.J. Bain, D. Berry, M. Krams, R. Sperling, D. Dilts, J. Luthman, D. Hanna, et al. 2015. Charting a path toward combination therapy for Alzheimer's disease. *Expert Rev. Neurother.* 15:107–113. https://doi.org/10.1586/14737175.2015.995168

Stern, E.A., B.J. Bacskai, G.A. Hickey, F.J. Attenello, J.A. Lombardo, and B.T. Hyman. 2004. Cortical synaptic integration in vivo is disrupted by amyloid-beta plaques. *J. Neurosci.* 24:4535–4540. https://doi.org/10.1523/JNEUROSCI.0462-04.2004

Stokin, G.B., C. Lillo, T.L. Falzone, R.G. Brusch, E. Rockenstein, S.L. Mount, R. Raman, P. Davies, E. Masliah, D.S. Williams, and L.S. Goldstein. 2005. Axonopathy and transport deficits early in the pathogenesis of Alzheimer's disease. *Science.* 307:1282–1288. https://doi.org/10.1126/science.1105681

Talboom, J.S., R. Velazquez, and S. Oddo. 2015. The mammalian target of rapamycin at the crossroad between cognitive aging and Alzheimer's disease. *NPJ Aging Mech. Dis.* 1:15008. https://doi.org/10.1038/npjamd.2015.8

Tsai, J., J. Grutzendler, K. Duff, and W.B. Gan. 2004. Fibrillar amyloid deposition leads to local synaptic abnormalities and breakage of neuronal branches. *Nat. Neurosci.* 7:1181–1183. https://doi.org/10.1038/nn1335

Ulrich, J.D., J.M. Burchett, J.L. Restivo, D.R. Schuler, P.B. Verghese, T.E. Mahan, G.E. Landreth, J.M. Castellano, H. Jiang, J.R. Cirrito, and D.M. Holtzman. 2013. In vivo measurement of apolipoprotein E from the brain interstitial fluid using microdialysis. *Mol. Neurodegener.* 8:13. https://doi.org/10.1186/1750-1326-8-13

Venables, W.N., and B.D. Ripley. 2002. Modern Applied Statistics with S. Fourth edition. Springer-Verlag, New York. 497 pp.

Walsh, D.M., I. Klyubin, J.V. Fadeeva, W.K. Cullen, R. Anwyl, M.S. Wolfe, M.J. Rowan, and D.J. Selkoe. 2002. Naturally secreted oligomers of amyloid beta protein potently inhibit hippocampal long-term potentiation in vivo. *Nature.* 416:535–539. https://doi.org/10.1038/416535a

Wang, A., P. Das, R.C. Switzer III, T.E. Golde, and J.L. Jankowsky. 2011. Robust amyloid clearance in a mouse model of Alzheimer's disease provides novel insights into the mechanism of amyloid-beta immunotherapy. *J. Neurosci.* 31:4124–4136. https://doi.org/10.1523/JNEUROSCI.5077-10.2011

Wong, G.T., D. Manfra, F.M. Poulet, Q. Zhang, H. Josien, T. Bara, L. Engstrom, M. Pinzon-Ortiz, J.S. Fine, H.J. Lee, et al. 2004. Chronic treatment with the gamma-secretase inhibitor LY-411,575 inhibits beta-amyloid peptide production and alters lymphopoiesis and intestinal cell differentiation. *J. Biol. Chem.* 279:12876–12882. https://doi.org/10.1074/jbc.M311652200

Youmans, K.L., S. Leung, J. Zhang, E. Maus, K. Baysac, G. Bu, R. Vassar, C. Yu, and M.J. LaDu. 2011. Amyloid-β42 alters apolipoprotein E solubility in brains of mice with five familial AD mutations. *J. Neurosci. Methods.* 196:51–59. https://doi.org/10.1016/j.jneumeth.2010.12.025

Zeileis, A. 2004. Econometric computing with HC and HAC covariance matrix estimators. *J. Stat. Softw.* 11:1–17. https://doi.org/10.18637/jss.v011.i10

Zhang, Y.D., and J.J. Zhao. 2015. TFEB participates in the Abeta-induced pathogenesis of Alzheimer's disease by regulating the autophagy-lysosome pathway. *DNA Cell Biol.* 34:661–668. https://doi.org/10.1089/dna.2014.2738

Zhang, W., J. Hao, R. Liu, Z. Zhang, G. Lei, C. Su, J. Miao, and Z. Li. 2011. Soluble Aβ levels correlate with cognitive deficits in the 12-month-old APPswe/PS1dE9 mouse model of Alzheimer's disease. *Behav. Brain Res.* 222:342–350. https://doi.org/10.1016/j.bbr.2011.03.072